Photopyroelectric spectroscopy and calorimetry

D. Dadarlat[1], C. Tripon[1]*, Iain R. White[2], Dorota Korte[2]

[1]National Institute for R&D of Isotopic and Molecular Technologies, 67-103 Donat str., 400293 Cluj-Napoca, Romania
[2]Laboratory for Environmental and Life Sciences, University of Nova Gorica, Vipavska 13, 5000 Nova Gorica, Slovenia

Corresponding author e-mail address: carmen.tripon@itim-cj.ro

ABSTRACT. In this tutorial, we present an overview of the development of the photopyroelectric (PPE) technique, from its beginnings in 1984, through to the present day. The tutorial is organized in five sections, exploring both theoretical and experimental aspects of PPE detection, as well as some important spectroscopic and calorimetric applications. In the "Introduction" section we present the fundamental basics of photothermal phenomena and the state-of-the-art of the photopyroelectric technique. In the "Theoretical aspects" section we describe some specific cases of experimental interest, with examples in both back and front detection configurations. Several mathematical expressions for the PPE signal in specific detection modes (combined back-front configurations and PPE-IRT methods) are also deduced. The "Instrumentation and experiment" section contains two sub-sections. The first describes several examples of set-ups used for both room temperature and temperature-controlled experiments. The second sub-section is dedicated to the configuration of detection cells and to the various sensor/sample assemblies that are currently used in spectroscopic and calorimetric experiments for both liquid and solid samples. The "Applications" section is in fact a collection of experimental results dedicated to the thermal characterization of a wide range of solid and liquid samples. At the end of this section we present some examples that have been selected to convey that the PPE technique is not only useful in the investigation of optical and thermal properties of a variety of condensed matter samples, but also to study physical and chemical processes such as molecular associations, food adulteration or phase transitions. In "Concluding remarks" we summarize the advantages of this technique in spectroscopic and calorimetric applications.

Keywords: photopyroelectric spectroscopy; photopyroelectric calorimetry; phase transitions; condensed matter samples; thermal parameters.

1. INTRODUCTION

The development of photothermal (PT) methods began in the '80s, due to the emerging opportunities being offered by laser and radiation detection techniques. Since then, the main discussion forum of the international scientific community in this field has been the "International Conference on Photothermal and Photoacoustic Phenomena", organized each second year. Often, Gordon type research conferences were organized on this topic and held on alternate years. Since 1981, there have been 21 international conferences on photoacoustic and photothermal phenomena, and 8 Gordon research conferences. The most recent of which was the ICPPP21.

Concerning the development of this field of research, after passing through the stages of experimental demonstration and fundamental theory, effort is now placed on optimizing experimental configurations of PT techniques towards quantitative analysis of the thermo-optical properties of materials. The compatibility of PT techniques with a large class of materials has been proved. This includes homogeneous materials with well-defined properties, as well as inhomogeneous materials with complex structures, such as composite materials, foodstuff, agricultural and biological products, drugs, building materials, etc.

All PT techniques are based on the same principle: a sample is irradiated with optical light and part of this radiation is absorbed by the sample and transformed into heat. If the heat absorbed into the sample and its propagation are measured, then optical or thermal information about the sample is obtained. The main information obtained with PT techniques are: - *thermal properties* (specific heat, thermal conductivity, diffusivity and effusivity, coefficients of thermal exchange, etc.); - *optical properties* (surface and volume optical absorption coefficient, reflection and diffusion coefficients, etc.); and - *quantum properties* (fluorescence and radiation to heat conversion efficiency). Each way of measuring the heat developed in the sample is practically associated with a PT method. The main photothermal techniques comprise: the photopyroelectric method, thermal lensing, infrared radiometry, the photothermal displacement method, photothermal beam deflection, and several others.[1] Amongst these methods, the photopyroelectric (PPE) technique is probably the simplest, because the temperature variation of the sample is directly measured with a pyroelectric sensor. The first PPE experiments were performed in 1984.[2–4] The targets of the investigations were very different: either to detect a phase transition, to study a chemical reaction, or to find the optical absorption bands of certain solids. This wide range in applications demonstrated early on that the PPE method is suitable for both spectroscopic and calorimetric investigations.

The PPE method is practically based on the pyroelectric effect i.e., the induction of spontaneous polarization in a non-centrosymmetric piezoelectric crystal, as a result of a temperature change in the crystal. The pyroelectric effect was discovered in antiquity, but the physical processes behind pyroelectricity were only studied at the end of 18th Century by William Thomson (Lord Kelvin), Woldemar Voigt and the Curie brothers[5, 6]. Nowadays, single crystals such as $LiTaO_3$ and TGS, ceramics such as PZT, or polymers such as PVDF are used as pyroelectric sensors.

Essentially the PPE method is based on the following principle: temperature variation in a sample exposed to modulated radiation is measured with a pyroelectric sensor, situated in close thermal contact with the sample.[7, 8] The main advantages of this technique include its simplicity, high sensitivity, non-destructive character and adaptability to practical restrictions imposed by the experimental requirements.

From a theoretical point of view, in the most general case, the complex PPE signal depends on all optical and thermal parameters of the layers of the detection cell (of which there are usually six: air, the window, the sample, the pyroelectric sensor, the substrate and the backing) and on several instrumental parameters (the modulation frequency of radiation, the power of the laser beam, the electrical capacity and permittivity of the sensor, etc.). Unfortunately, the mathematical expression of the PPE signal is very complicated, rendering it impractical for most applications. As a result, over the last few decades a large effort was dedicated to simplifying it, with focus on the number of components of the detection cell and on the thermal and optical thickness of each layer. As a final result, several specific modes were obtained, in which information is contained in both the amplitude and phase of the complex PPE signal.[7–9]

If the wavelength of the radiation source is scanned in a PPE experiment, spectroscopic information (mainly optical absorption coefficients) can be obtained. If the wavelength of the radiation source is constant, the PPE technique practically becomes calorimetry and experimental investigation yields thermal information (static and dynamic thermal parameters). The thermal parameters directly obtained from PPE measurements are usually the "fundamental" ones, namely the thermal diffusivity and effusivity (which are also present in the thermal diffusion equation and its solution). It is well known that the four thermal parameters, the static volume specific heat *(C)*, the dynamic thermal diffusivity *(α)*, conductivity *(k)*, and effusivity *(e)*, are connected by two relationships, $k=C\cdot\alpha$ and $e=(C\cdot k)^{1/2}$. Thus only two parameters are independent.

Recently, it was demonstrated that PPE spectroscopy is able, in certain detection modes, to offer both spectroscopic and calorimetric information.[10] Concerning PPE detection configurations, two of them, "back" and "front", have mostly been applied to spectroscopic/calorimetric studies, respectively. Some spectroscopic information has also been obtained from a so-called "reflection mode" PPE configuration. In the back (standard) configuration, a modulated light impinges on the front surface of a sample, and a pyroelectric sensor, situated in good thermal contact with the sample's rear side, measures the heat developed in the sample due to the absorption of radiation.[9, 11] In the front (inverse) configuration, radiation impinges on the front surface of the sensor, and the sample, in good thermal contact with its rear side, acts as a heat sink.[12, 13] The reflection mode PPE configuration is in fact a back configuration with a (semi)transparent sample and a very reflective sensor.[14]

Concerning the types of samples that can be investigated, in general the PPE method can be successfully applied to condensed matter (liquids and solids). Liquids are the most suitable materials for PPE investigation, because sample-sensor thermal contact is perfect in most cases, leading to accurate, quantitative results. For solid samples, the method can be readily applied, but the sample-sensor coupling fluid (that is almost always necessary) may introduce uncontrolled errors. PPE calorimetry can also be used for gases but only under very special conditions due to their low optical absorption coefficients and large thermal diffusion lengths.

Historically speaking, in PPE calorimetry many different approaches have been developed to obtain values of thermal parameters. Some of them are based on the measurement of single values[13, 15]; whilst other alternatives make use of scanning procedures.[9, 11, 15] The second approach proves to be more precise. When liquid samples are under investigation, two parameters are available to be scanned: the chopping frequency of radiation and the sample's thickness.

In principle, several combinations can be selected by the researcher, in order to obtain at least one of the dynamic thermal parameters related to a sample (thermal diffusivity or effusivity). The combinations refer to the detection configuration (back or front), the source of

information (PPE amplitude or phase) and the scanning parameter (chopping frequency or a sample thickness scan).

To conclude this introduction we must highlight that optical and thermal parameters are markers in many physical/chemical processes. Consequently, the PPE method is a very suitable technique to not only determine values of optical and thermal parameters but also study processes such as: compositional changes (chemical reactions, mixtures of liquids, molecular and/or isotopic association, food adulteration, etc.), structural/magnetic/electric changes induced by temperature variation (phase transitions), and more.

In this tutorial we intend to present an overall view of the development of the PPE technique, starting from 1984, until now. This review is organized into three main sections, to explore both theoretical and experimental aspects of PPE detection, as well as providing important examples of spectroscopic and calorimetric applications. In the theoretical section we describe some specific detection cases of experimental interest, in both back and front configurations. The experimental section contains examples of set-ups, detection cells' configurations and various sensor/sample assemblies that are used in both spectroscopic and calorimetric experiments. The section dedicated to applications contains a selection of case studies that cover a wide variety of scientific disciplines and research fields. We intend to show that the PPE technique is not only useful to investigate optical and thermal properties of various solids (homogeneous and porous, magnets, ferroelectrics, thermoelectrics, etc.) and liquids (binary and isotopic mixtures, volatile liquids, liquid foodstuffs, magnetic nanofluids, etc), but simultaneously provides a good method to study physical processes (such as molecular associations, food adulteration or phase transitions).

The reader should be made aware that it is impossible to encompass the whole activity in this field, that extends over more than 35 years, within a single paper; this review therefore often focuses on the activity of the author's group and co-workers. However, the extended list of references represents a wealth of important results that have been obtained by other groups that are activate in this field.

2. THEORETICAL ASPECTS

The starting point in developing the theory of the PPE method is the relationship between the PPE voltage V, and the temperature variation ΔT, across the pyroelectric sensor. It was demonstrated[7, 8] that for low levels of irradiation the two quantities are proportional, $V = p \cdot \Delta T$, p being the pyroelectric coefficient of the sensor. From a theoretical point of view, the target is to calculate ΔT by solving a system of heat diffusion equations through the layered detection cell, with boundary conditions of temperature and flux continuity at interfaces. On the other hand, it is now well known that the general expression for the PPE signal is analytically exact[7, 8] but, as mentioned in the introduction, it is too complicated for experimental applications. This is why, in this theoretical section, we will not describe the development of the general PPE theory; we will limit our presentation to mathematical equations of the complex PPE signal used in several specific detection cases of the two most commonly applied detection configurations (back and front).

One-directional heat propagation is based on the concept of thermal waves and several parameters characterizing light propagation have corresponding parameters in heat propagation. As with the case of optics and light, thermal waves are attenuated when propagating into a given material. In analogy with the optical penetration depth, in heat propagation the thermal diffusion length, μ, is defined as the heat penetration distance for which the thermal wave is attenuated with a factor of "e". In frequency dependent experiments, the thermal diffusion length depends on the material's thermal diffusivity and on the modulation

frequency of incident radiation (see Eq. (4)). When the frequency of modulated light increases, the thermal diffusion length decreases; which is in fact a method of manipulating the thermal thickness of a given layer of the detection cell. Often, in real experiments, we are obliged to assign various layers of the detection cell as either "thermally thin" or "thermally thick". This means that sometimes we like to let the heat to pass through a given layer of the detection cell almost non-attenuated (a thermally thin layer) or we want all (or most) of the heat to be absorbed in the layer (a thermally thick layer). From a theoretical point of view the critical frequency at which a layer passes from a thermally thin to a thick regimen is obtained when the geometrical thickness of the layer, L, is equal with the thermal diffusion length, μ. Thermally thin/thick concepts are in fact connected with approximations that are required in the development of theoretical aspects. Approximations that are made when $1 << L/\mu$, or $L/\mu >> 1$ lead to simplified theoretical results that are of experimental interest.

Several assumptions (restrictions) must be made from the beginning for the sake of simplification. These assumptions are general in nature and it is easy to set them up experimentally. They are: *(i)* that a one-dimensional propagation of heat is considered; *(ii)* that heat transport is due only to conduction (heat transport by radiation and convection is neglected). However, under special experimental conditions, these latter two heat transfer mechanisms can be also considered.[16–18] In the following sections we will describe, from a theoretical point of view, some specific PPE detection cases of experimental interest. Additional restrictions will be imposed in each particular case.

2.1.PPE Spectroscopy

As described in the previous section, the general expression for the PPE signal is analytically rather complicated. It depends on the optical and thermal parameters of all layers of the detection cell, together with others parameters that characterize the set-up. For practical reasons, many of these parameters are eliminated by performing various approximations or normalization procedures. The main difference between spectroscopic and calorimetric applications is the sample transparency. In calorimetric applications (which will be presented later in section 4) the sample (or the sensor, in front configuration) is opaque and all radiation is absorbed by the irradiated surface. In spectroscopic applications the sample is (semi)transparent and the PPE signal depends on the optical absorption coefficient of the sample. There are many analytical expressions of the PPE signal used in spectroscopic applications. We will not list them here, but interested readers can find more information in Refs. [7] and [8].

2.2.PPE Calorimetry

2.2.1. Back Configuration

A typical geometry of the back PPE configuration is presented in Fig.1 [7, 8, 19, 30].

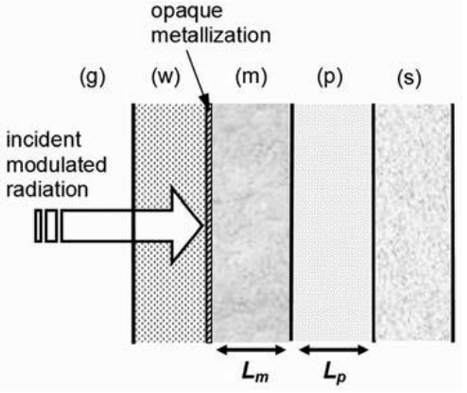

Fig. 1. Schematic view of the PPE detection cell in back configuration.[30]
Reprinted from Dadarlat, D.; Neamtu, C. Acta Chim. Slov. 56(1), 225-236, 2009; licensed under a Creative Commons Attribution (CC BY) license.

For this geometry, the system of thermal diffusion equations can be written as:

$$\frac{d^2T_i}{dx_i^2} - \frac{i\omega}{\alpha_i}T_i = 0; \quad i = g, w, m, p, s \tag{1}$$

with the boundary conditions of temperature and flux continuity at the interfaces:

$$T_i = T_j \qquad \text{(i, j) = (g, w), (w, m), (m, p), (p, s)}$$

$$k_i\frac{dT_i}{dx} - k_j\frac{dT_j}{dx} = 0 \qquad \text{(i, j) = (g, w), (m, p), (p, s)} \tag{2}$$

$$k_i\frac{dT_i}{dx} - k_j\frac{dT_j}{dx} = \frac{1-R}{2}H_0 \qquad \text{(i, j) = (w, m)}$$

In Eqs. (1) – (2) the term (1 – R) represents the quantity of the light intensity absorbed at the (w, m) interface and H_0 is the incident light intensity.

With the additional simplifying assumptions that the window and substrate are thermally thick (their geometrical thickness is larger than the thermal diffusion length), the air and window are optically transparent, and the incident radiation is absorbed at the window-material interface (by a thin opaque layer), the PPE voltage is given by[19]:

$$V = \frac{2V_0 exp(-\sigma_m L_m)}{(b_{wm}+1)(b_{mp}+1)} \cdot \frac{exp(\sigma_p L_p)+R_{sp}exp(-\sigma_p L_p)-(1+R_{sp})}{\exp(\sigma_p L_p)-R_{sp}R_{mp}exp(-\sigma_p L_p)+[R_{mp}exp(\sigma_p L_p)-R_{sp}exp(-\sigma_p L_p)R_{wm}exp(-2\sigma_m L_m)]} \tag{3}$$

where

$$R_{jk} = (b_{jk}-1)/(b_{jk}+1); \quad b_{jk} = e_j/e_k; \quad \sigma_j = (1+i)a_j; \quad \mu = (2\alpha/\omega)^{1/2} \tag{4}$$

In Eq. (3), V_0 is an instrumental factor, R_{jk} represents the reflection coefficient of the thermal wave at the '*jk*' interface, ω is the angular chopping frequency and σ and a are the complex

thermal diffusion coefficient and the reciprocal of the thermal diffusion length ($a = \mu^{-1}$), respectively.

In order to eliminate V_0, normalization of the signal is necessary, the best reference signal being obtained by direct irradiation of the empty sensor.

The obtained normalized signal is:

$$V_n(f) = \frac{2(b_{gp}+1)}{(b_{wm}+1)(b_{mp}+1)} exp(-\sigma_m L_m) P(f) \tag{5}$$

where

$$P(f) = \frac{1-R_{sp}R_{gp}exp(-2\sigma_p L_p)}{1-R_{sp}R_{mp}exp(-2\sigma_p L_p)+[R_{mp}-R_{sp}exp(-2\sigma_p L_p)]R_{wm}exp(-2\sigma_m L_m)} \tag{6}$$

If we work in the thermally thick regime for the sensor ($L_p >> \mu_p$) and we extract the phase and the amplitude from Eq. (5), we get for the phase:

$$\Theta = -\arctan\left[\frac{\sin(a_m L_m) - R\,e^{-2a_m L_m})[\sin(a_m L_m)\cos(2a_m L_m) - \cos(a_m L_m)\sin(2a_m L_m)]}{\cos(a_m L_m) - R\,e^{-2a_m L_m})[\sin(a_m L_m)\sin(2a_m L_m) + \cos(a_m L_m)\cos(2a_m L_m)]}\right] \tag{7}$$

with $R = R_{mw}R_{mp}$, and for the amplitude:

$$\ln(|V_n|) = \ln(\frac{2(b_{gp}+1)}{(b_{wm}+1)(b_{mp}+1)}) - L_m a_m \tag{8}$$

An analysis of Eq. (7) indicates that the sample's thermal diffusivity (contained in a_m) can be directly measured by performing a frequency and/or a sample thickness scan of the phase of the PPE signal. The most suitable specific case seems to be the thermally thick regime for the sample, ($L_m >> \mu_m$), when Eq. (7) reduces to:

$$\Theta = \Theta_0 - L_m(\frac{\omega}{2\alpha_m})^{1/2} \tag{9}$$

leading to:

$$\alpha_m = \frac{\pi f L_m^{\,2}}{(\Delta\Theta)^2} \tag{10}$$

At this stage, the thermal diffusivity can be obtained using the slope of the curves $\Theta = \Theta(f^{1/2})$ or $\Theta = \Theta(L_m)$. This method is a direct one, and involves no calibration. Historically, the frequency scan was mainly used, probably due to the fact that it could be applied to both solid and liquid samples. However, when accurate measurements are necessary, exact knowledge of the sample thickness can be a problem, especially in the case of liquids. This is why methods based on a variable sample-to-source distance (with a so called thermal-wave resonator cavity, TWRC) were introduced.[17, 20–31] In such a method, the chopping frequency is kept constant, and a (liquid) sample thickness scan of the PPE signal's phase is performed. The advantage of

this method is that data processing does not require exact knowledge of the sample thickness, but only the sample thickness variation.

In Eq. (8), the amplitude of the PPE signal is the source of information. The sample's thermal diffusivity can be found from the slope of the PPE amplitude vs. $(f)^{1/2}$ or L_m, by following a similar procedure as in the case of the phase. If the value of the thermal diffusivity is known, Eq. (8) offers the possibility to measure the sample's thermal effusivity, preceded by a calibration with a reference liquid. If we denote the reference liquid by "*r*", we have for the normalized signal[32]:

$$\ln(|V_n|) = \ln\left(\frac{(b_{wr}+1)(b_{rp}+1)}{(b_{wm}+1)(b_{mp}+1)}\right) - L_m(a_r - a_m) \tag{11}$$

If y_0 is the value of the free term in Eq. (11), we obtain for the sample's thermal effusivity e_m the following equation:

$$e_p^{-1}e_m^2 + \left[\left(1 + e_w e_p^{-1}\right) - 2|V_n|^{-1}\left(1 + e_r e_p^{-1}\right)exp(-y_0)\right]e_m + e_w = 0 \tag{12}$$

2.2.2. *Front Configuration*

In order to deduce the theoretical equations for specific detection cases in the front configuration (FPPE), we consider the same geometry illustrated in Fig. 1, but without the material layer, "*m*". In this case, the front opaque electrical contact of the sensor is directly irradiated, and the substrate "s" plays the role of sample. Considering the same restrictions of a thermally thick window and substrate, the PPE voltage is given by[33]:

$$V = \frac{V_0}{(b_{wp}+1)} \cdot \frac{1-exp(-\sigma_p L_p)+R_{sp}[exp(-2\sigma_p L_p)-exp(-\sigma_p L_p)]}{1-R_{wp}R_{sp}exp(-2\sigma_p L_p)} \tag{13}$$

As in the case of the back configuration, in order to eliminate the instrumental factor V_0, a normalization procedure is necessary. The best reference signal is obtained with air instead of substrate. Assuming that R_{sp}= R_{gp}= -1, for the normalized signal one obtains:

$$V_n = 1 - \left(1 + R_{sp}\right)exp\left(-\sigma_p L_p\right) \tag{14}$$

If we extract the phase and amplitude from Eq. (14), we obtain for the phase:

$$\theta = arctg\,\frac{(1+R_{sp})sin(a_p L_p)exp(-a_p L_p)}{1-(1+R_{sp})cos(a_p L_p)exp(-a_p L_p)} \tag{15}$$

and for the amplitude:

$$|V_n| = \left\{\left[(1+R_{sp})sin(a_pL_p)exp(-a_pL_p)\right]^2 + \left[1-(1+R_{sp})cos(a_pL_p)exp(-a_pL_p)\right]^2\right\}^{1/2} \quad (16)$$

If the expression for the amplitude seems to be rather complicated for experimental measurements, the phase of the PPE signal can easily be used in order to obtain the thermal effusivity of the sample (or substrate in this case). From Eq. (15), R_{sp} can be derived as:

$$R_{sp} = \frac{tan(\theta)}{[sin(a_pL_p)+cos(a_pL_p)tan(\theta)]exp(-a_pL_p)} - 1 \quad (17)$$

and the sample's thermal effusivity as:

$$e_s = e_p\left(\frac{1+R_{sp}}{1-R_{sp}}\right) \quad (18)$$

For practical applications, a frequency scan of the phase of the signal is performed and the thermal effusivity is hence obtained by optimizing the fit performed on the experimental data with Eq. (17), considering e_s as a fitting parameter.

In this configuration, the amplitude has also been used (in the thermally thin regime for the sensor) to obtain single values of the sample's thermal effusivity.[34] However, in recent years it was mainly used to obtain information about the thermal properties of pyroelectric sensors.[35–37]

2.2.3. Special cases. Combined front/back configurations

Special detection configurations are usually related to the analysis of solid (especially porous) samples. When investigating solids, a coupling fluid (liquid or paste) is used between the sensor and sample, in order to ensure a good thermal contact. Often, especially when the target of the investigation refers to qualitative data, the influence that the coupling fluid may have on the results was neglected: experimental parameters (such as the sample and sensor thickness, modulation frequency of incident radiation, etc.) were designed in such a way that the coupling fluid layer was considered to be thermally very thin. Unfortunately, when accurate quantitative data are required, the influence of the coupling fluid cannot be neglected and much work was dedicated to reduce its influence. Several authors tried select the most appropriate coupling fluids and attempted to find mechanical methods to reduce their thickness.[38] Others elaborated mathematical models in which they included a layer of coupling fluid in a detection sandwich (i.e., sample/coupling fluid/sensor). In this case, the main problem is the unknown thickness of the coupling fluid, which is treated as a fitting parameter.[39, 40] Another method to eliminate the influence of the coupling fluid was to use the aforementioned thermal-wave resonator cavity (TWRC) method[20–31] in which a frequency scanning procedure is replaced by a coupling fluid thickness scan.

Even if the influence of the coupling fluid were reduced, the methods described above are only suitable for the investigation of non-porous solids. For porous solids, any type of liquid or pasty coupling fluid can infiltrate the sample and make the results less accurate. The only other option available for thermal studies of porous samples with PPE, is to replace the liquid/pasty coupling fluid between the sensor and sample with a layer of air. Unfortunately, if one decides to use air as a coupling fluid between the two solids (the sensor and the porous solid sample), the following additional problems must be dealt with: (i) air is a bad thermal conductor, acting

as a low pass filter in frequency dependent measurements and as a consequence an adequate experimental frequency range must be selected; (ii) the thickness of the air gap is unknown – meaning that it must be considered to be a fitting parameter or, if possible, it must be eliminated from the final result by some self-normalization method; (iii) sometimes, due to rather poor heat conduction in the layered detection cell, heat losses by convection and radiation at the heat-absorbent surface are indicated to be included in the model.

Now that we have described the challenges associated with the thermal investigation of porous solids, we will now describe two methods that can be used for such a purpose. The first, proposed by Salazar et al.,[18] is based on a frequency scan of the phase of the FPPE signal. This method uses a front detection configuration that takes into account heat losses from convection and radiation at the irradiated surface. It uses thin opaque pyroelectric sensors and leads to the direct measurement of the sample thermal effusivity, by performing a fit of the experimental data (FPPE phase vs. modulation frequency) with three fitting parameters: the sample thermal effusivity, heat losses from convection and radiation, and the air gap thickness between the sensor and sample. The second method, proposed by Zammit et al.,[41] is in fact a combined BPPE/FPPE configuration. It is based on two successive measurements (frequency scans), one in back and one in front configuration, followed by a self-normalization of the phase vs. modulation frequency behavior. The method uses transparent pyroelectric sensors, and the self-normalized PPE phase depends only on the sample thermal effusivity and diffusivity and on the thermal effusivity of the backing material (the phase of the signal is independent of the thermal and geometrical parameters of the sensor and coupling fluid between sensor and sample). This method allows the direct measurement of the sample thermal effusivity in the low frequency regime provided the thermal diffusivity has already been measured in the high frequency region.

PPE detection cells used in the two methods are schematically depicted in Fig 2.

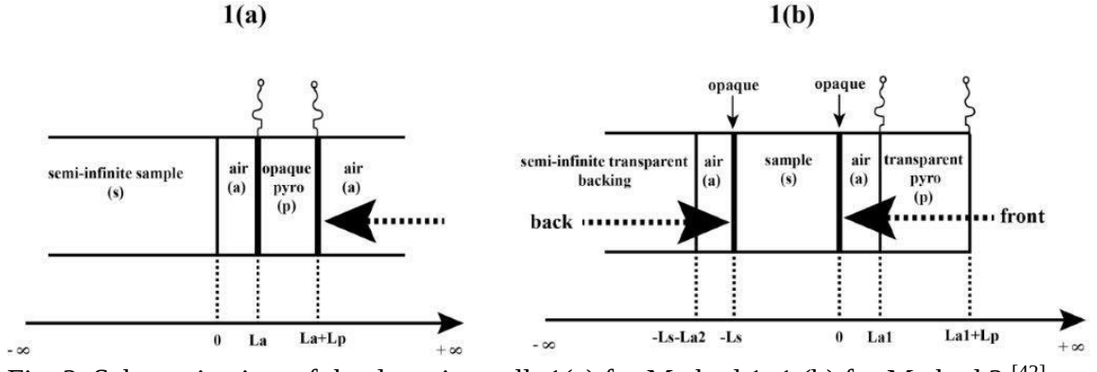

Fig. 2. Schematic view of the detection cell: 1(a) for Method 1, 1 (b) for Method 2.[42] Reproduced with permission from Thermochim. Acta. 702, 178943 (2021). Copyright 2021 Elsevier.

In the first method, the normalized FPPE signal (normalization performed with the sensor and without sample) is described by the following relationship (where the coupling fluid and the backing material have already been replaced by air) [18, 42]:

$$V_n = \frac{2A0(A1 + A2)}{B1\cosh(q_a L_a) + B2\sinh(q_a L_a)} \tag{19}$$

where:

$$A0 = \left(1 + \frac{h}{e_a\sqrt{i\omega}}\right)\cosh\left(\frac{q_p L_p}{2}\right) + \frac{e_p}{e_a}\sinh\left(\frac{q_p L_p}{2}\right) \tag{20}$$

$$A1 = \frac{e_p}{e_a}\cosh\left(\frac{q_p L_p}{2}\right)\left(\cosh(q_a L_a) + \frac{e_s}{e_a}\sinh(q_a L_a)\right) \tag{21}$$

$$A2 = \sinh\left(\frac{q_p L_p}{2}\right)\left(\frac{e_s}{e_a}\cosh(q_a L_a) + \sinh(q_a L_a)\right) \tag{22}$$

$$B1 = \frac{e_p}{e_a}\left(1 + \frac{e_s}{e_a} + \frac{h}{e_a\sqrt{i\omega}}\right)\cosh(q_p L_p) + \left[\left(\frac{e_p}{e_a}\right)^2 + \frac{e_s}{e_a}\left(1 + \frac{h}{e_a\sqrt{i\omega}}\right)\right]\sinh(q_p L_p) \tag{23}$$

$$B2 = \frac{e_p}{e_a}\left[1 + \frac{e_s}{e_a}\left(1 + \frac{h}{e_a\sqrt{i\omega}}\right)\right]\cosh(q_p L_p) + \left[1 + \frac{h}{e_a\sqrt{i\omega}} + \left(\frac{e_p}{e_a}\right)^2\frac{e_s}{e_a}\right]\sinh(q_p L_p) \tag{24}$$

In Eqs. (19) - (24) e_i and L_i represent the thermal effusivity and geometrical thickness of the „*i*" layer, $\omega = 2\pi f$ is the angular modulation frequency, $q_i = (\omega/\alpha_i)^{1/2}$, where α_i represents the thermal diffusivity of the „*i*" layer. The thermal diffusivity and effusivity of air are well-known: e_a = 5.5 $Ws^{1/2}/m^2K$ and $\alpha_a = 21x10^{-6}$ m^2/s. Consequently Eq. (19) can be used to fit an experimental scan V_n vs. modulation frequency „*f*", with the sample's thermal effusivity, e_s, heat losses from convection and radiation, *h*, and the air gap thickness between the sensor and sample, L_a, as fitting parameters. It has been demonstrated in certain cases, the three parameters are almost independent and thus the solution of the fit can be unique.[19, 43]

Concerning the second method (Fig. 2b) it is based on two successive frequency scans, one in back and one in front PPE configuration, followed by a self-normalization of the phase vs. modulation frequency behaviors (phase BPPE/phase FPPE). The self-normalized phase of the PPE signal is given by the relationship:[41, 42]

$$\varphi = -a_s L_s + tan^{-1}\left(\frac{(1 - b_{bs})sin(2a_s L_s)exp(-2a_s L_s)}{(1 + b_{bs}) + (1 - b_{bs})cos(2a_s L_s)exp(-2a_s L_s)}\right) \tag{25}$$

where

$$b_{bs} = \frac{e_b}{e_s}; a_s = \sqrt{\frac{\pi f}{\alpha_s}} \tag{26}$$

Eq. (25) indicates that for high enough modulation frequencies the second term from the right side vanishes and one can easily obtain the sample's thermal diffusivity. In principle by using its value in Eq. (25) in the low frequency range, one can obtain the sample's thermal effusivity via a fitting procedure. An analysis of Eq. (25) shows that if the backing material is air, we can approximate b_{bs}=0 and Eq. (25) takes the simplified form:

$$\varphi = -a_s L_s + tan^{-1}\left(\frac{sin(2a_s L_s)}{exp(2a_s L_s) + cos(2a_s L_s)}\right) \tag{27}$$

Eq. (27) shows that in using air as a backing material with this configuration, one can only measure the sample's thermal diffusivity, both in low and high frequency range.

Combining both previously described methods[18, 41] we can obtain both the thermal diffusivity and effusivity of a porous sample and subsequently calculate the remaining thermal parameters: the thermal conductivity and the volume specific heat, for complete thermal characterization of the material.

2.3.Combined PPE methods with other PT methods

The PPE method can be combined with other PT techniques in order to obtain a complete thermal characterization (i.e., the measurement of all thermal parameters) of condensed matter samples. Practically, when we combine two methods we try to utilise the particular advantages of each technique whilst simultaneously trying to eliminate their limitations. The PPE method has been combined with photothermal radiometry (PTR)[43–45], the photothermoelectric (PTE) method[46–53], the thermography (IRT), etc.[54–57]

To describe of all these mixed methodologies would take too much space and so we will limit our description to the theoretical aspects of the PPE-PTR approach only. Readers interested in other combinations are directed towards the references described above.

The PTR technique has mostly been used for calorimetric investigations of solid samples,[58, 59] with the frequency scan method. In such types of investigation the irradiated layer is a thermally thin and opaque solid, and normalization of the PTR signal involves a thermally thick backing with known thermal properties.

The layout of the PPE-PTR detection configuration is presented in Fig. 3.

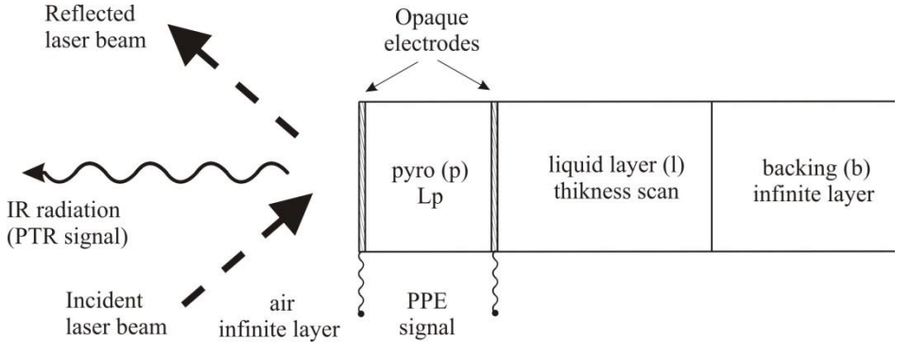

Fig. 3. Layout of the PPE-PTR detection configuration.[43] Reproduced with permission from Int. J. Thermophys. 31(11–12), 2275 (2010). Copyright 2010 Springer Science+Business Media.

Using the classical procedure described in [60], one can obtain for the PTR signal:

$$V^{PTR} = \frac{\Gamma}{2k_p\sigma_p}\frac{1+R_{lp}\exp(-2\sigma_p L_p)}{1-R_{lp}\exp(-2\sigma_p L_p)} \tag{28}$$

Where Γ is a dimensionless experimental parameter and

$$R_{lp} = \frac{1 - b_{lp} + R_{bl}(1 + b_{lp})\exp(-2\sigma_l L_l)}{1 + b_{lp} + R_{bl}(1 - b_{lp})\exp(-2\sigma_l L_l)} \tag{29}$$

For very thick liquid layer

$$\exp(-2\sigma_l L_l)=0 \text{ and } R_{lp}^{\infty} = \frac{1 - b_{lp}}{1 + b_{lp}} \tag{30}$$

and the normalization signal becomes:

$$V_{\infty}^{PTR} = \frac{\Gamma}{2k_p\sigma_p}\frac{1 + R_{lp}^{\infty}\exp(-2\sigma_p L_p)}{1 - R_{lp}^{\infty}\exp(-2\sigma_p L_p)} \tag{31}$$

Combining Eqs. (28)-(31), we obtain for the normalized PTR signal:

$$V_n^{PTR} = \frac{A_- B_+}{A_+ B_-} \tag{32}$$

where

$$A_{\pm} = 1 + b_{lp} \pm (1 - b_{lp})\exp(-2\sigma_p L_p) \tag{33}$$

$$B_{\pm} = \left\{1 + b_{lp} + R_{bl}(1 - b_{lp})\exp(-2\sigma_l L_l) \pm \left[1 - b_{lp} + R_{bl}(1 + b_{lp})\exp(-2\sigma_l L_l)\right]\exp(-2\sigma_p L_p)\right\}$$

As demonstrated previously, for the detection cell described in Fig. 3, the PPE signal in front configuration is given by the relationship:

$$V_n^{PPE} = \frac{\sigma_p L_p + b_{lp}}{(\sigma_p L_p) + b_{lp}\left[\frac{1 - R_{bl}\exp(-2\sigma_l L_l)}{1 + R_{bl}\exp(-2\sigma_l L_l)}\right]} \tag{34}$$

We can conclude that both normalized FPPE and PTR signals depend on the thermal diffusivity and effusivity of the pyroelectric sensor and the liquid layer respectively, and on the thermal effusivity of the backing material. Performing a thickness scan of the amplitude and/or phase of the FPPE and PTR signals (at constant chopping frequency) one can get information about one or eventually two layers of the detection cell.

The theoretical equations deduced here represent a small selection that describe particular cases of experimental interest. They will be used later in the section dedicated to Applications.

3. INSTRUMENTATION AND EXPERIMENT

3.1.EXPERIMENTAL SET-UP

3.1.1. PPE spectroscopy

A classical experimental set-up for PPE spectroscopy is presented in Fig. 4.

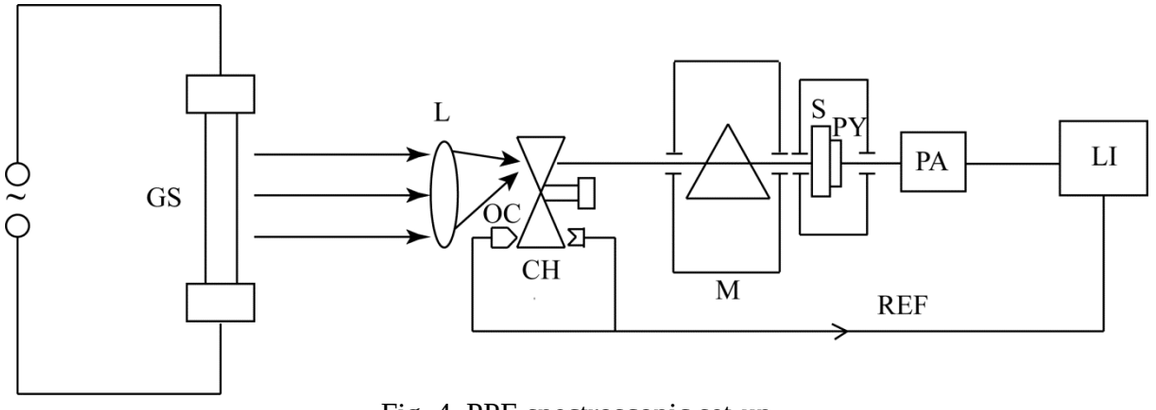

Fig. 4. PPE spectroscopic set-up

In PPE spectroscopy, radiation is emitted by a black-body radiation source at a temperature appropriate for the spectral range of interest. For the visible-infrared spectral range, the most common radiation source is the Globar (GS), which is a silicone-carbide bar at a temperature of about 1600 K, capable of covering the spectral range from 0.5 μm, up to about 20 μm. Radiation is collimated (lens L) and modulated with an electro-mechanical chopper (CH) before it passes through a prism monochromator (M). The radiation that exits the monochromator impinges on the sample's (S) incident surface. The rear side of the sample is in thermal contact with the pyroelectric sensor (PY). The PPE signal from the sensor is amplified (PA) and then processed with a selective or a lock-in nanovoltmeter (LI). The reference signal for the lock-in amplifier is obtained with an opto-coupler (OC) photodiode-phototransistor. With such a set-up, one can usually obtain the optical absorption bands of the samples in the spectral range of interest.

If additional information is needed (for example one is also interested in the reflection coefficient of the sample) another detection line can be added to the set-up from Fig. 4. (see Fig. 5). The reflected radiation from the sample can be collected with a second pyroelectric sensor (RD) and the signal processed with a second lock-in.[61]

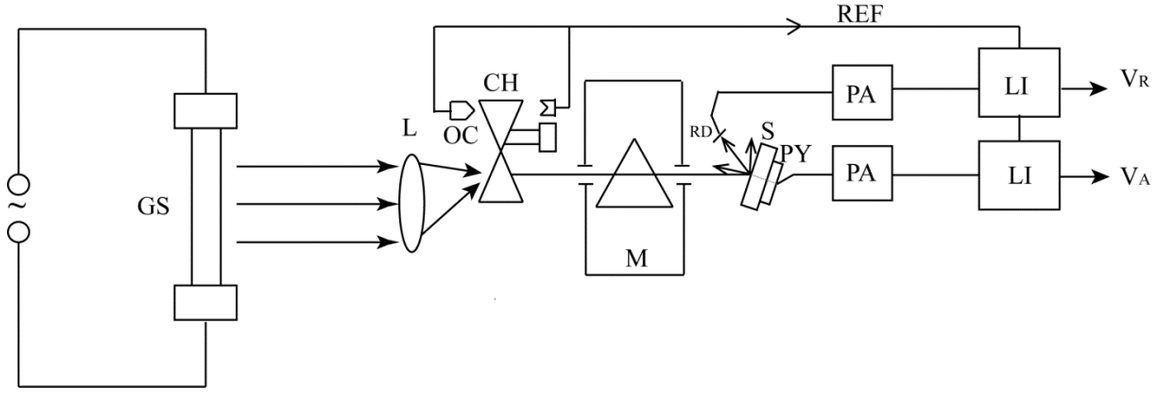

Fig. 5. PPE set-up for differential spectroscopy. (GS - Globar source, L - quartz lens, CH - chopper, M – monochromator, PZT – pyroelectric sensor, PA – preamplifiers, S – sample, LI – lock-in, OC – opto-coupler, REF – reference signal, VA – PPE absorption signal, VR – PPE reflection signal).

Other experimental solutions can be found in Refs. [10, 62]

3.1.2. PPE calorimetry

A typical experimental set-up for the PPE measurement of thermal parameters for liquid samples at room temperature is displayed in Fig. 6.

In this set-up, a pyroelectric sensor, usually a 100 – 500 μm thick $LiTaO_3$ single crystal, provided with Cr-Au electrodes on both faces, is glued to a rotating stage. The backing material of the detection cell is situated on a micrometric stage. The modulated radiation (provided by a 30 - 200 mW laser) is partially absorbed by the front electrode of the sensor. The space between the sensor and the backing material accommodates a liquid layer. Variation in the thickness of the liquid is achieved with a step in the range 30 nm - 1 μm with a nano-motor and data acquisition is taken each 10^{th} - 30^{th} step. The "rough" control of the liquid's thickness and the parallelism between the backing and the sensor are assured by 3 and 6–axis micrometric stages. During the scanning procedure, the sample's thickness variation is rigorously controlled but the absolute sample thickness is not precisely known. The PPE signal is processed with a lock-in amplifier. The internal oscillator of the lock-in gives the reference signal and assures the modulation of the incident radiation. The data acquisition, processing and analysis are performed with appropriate software.

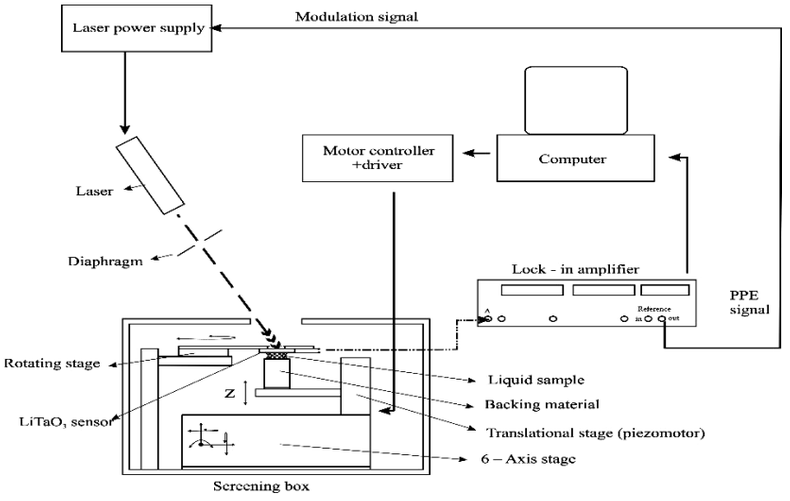

Fig. 6. PPE calorimetric set-up for investigations of thermal parameters at room temperature.[31] Reproduced with permission from Laser Phys. 19(6), 1330 (2009). Copyright (2009) IOP Publishing.

The set-up presented in Fig. 6 was specially designed for investigations of thermal parameters (mainly thermal effusivity) of liquids, and it is based on the TWRC method.[20–31] With minor changes in the design of the detection cell (see the section dedicated to detection cells) the very same experimental set-up can be used for PPE measurements of thermal diffusivity and can be applied to solid samples. In such a case, the TWRC method must be replaced by a classical frequency scanning procedure.

Fig. 7 presents an extended experimental set-up in which the PPE method is coupled with the PTR technique. In this improved set-up, a second lock-in amplifier is added which processes the signal provided by an IR detector. During such an experiment, a second IR signal is generated by the pyroelectric sensor itself. The IR radiation emitted by the pyroelectric sensor is collected with parabolic mirrors and diverted to the surface of a cooled HgCdTe IR detector. The internal oscillator of the lock-in used in PPE measurements also gives the reference signal for the second lock-in. The two PPE and PTR signals are processed with a computer.

The experimental set-ups described so far are useful for studies at room temperature. When temperature dependent processes must be studied, certain components must be added to allow temperature variation and control. A schematic view of such a set-up is presented in Fig. 8.

In Fig. 8, a radiation source, usually a laser, is modulated by an acoustic-optical modulator and the PPE signal is processed with a lock-in amplifier. When performing temperature scans (phase transition investigations, for example), a thermostat, provided with Peltier elements[64] with additional equipment (programmable power supply, electronic thermometer, etc.) for temperature control, is included in the set-up. A computer with appropriate software is used for data acquisition.

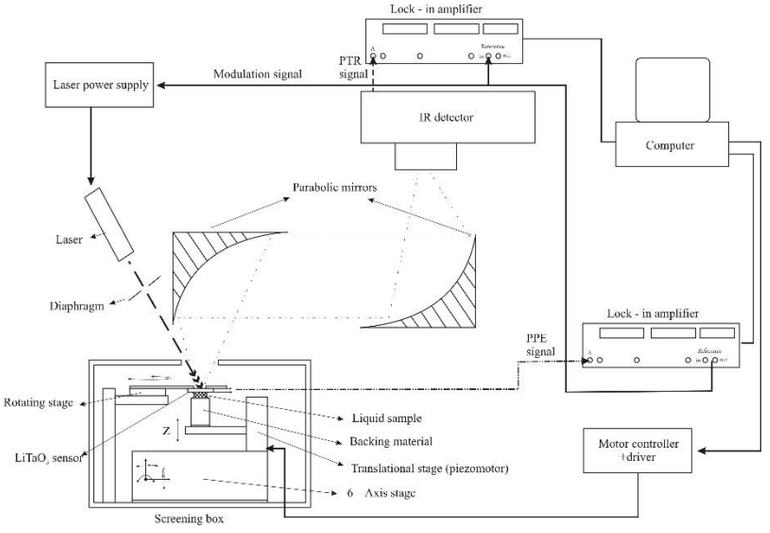

Fig. 7. Set-up for coupled PPE-PTR investigations.[44] Reproduced with permission from Int. J. Thermophys. 32 (10), 2092 (2011). Copyright 2011 Springer Science+Business Media.

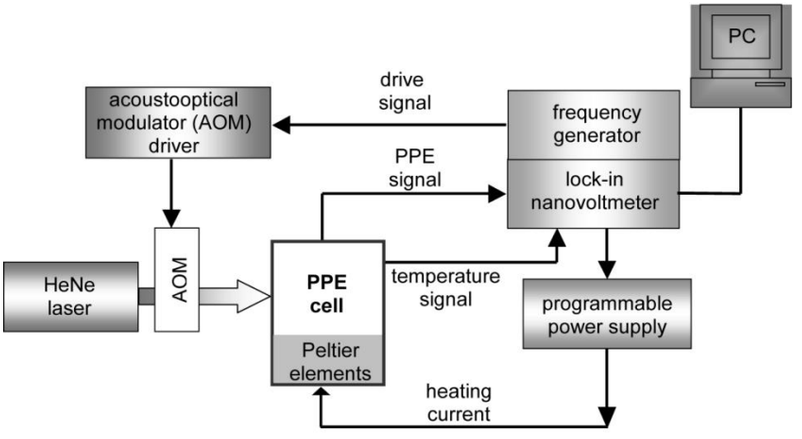

Fig. 8. Typical PPE set-up for investigations of temperature dependent processes.[30] Reprinted from Dadarlat, D.; Neamtu, C. Acta Chim. Slov. 56 (1), 225-236, 2009; licensed under a Creative Commons Attribution (CC BY) license.

3.2.DETECTION CELLS AND SENSOR-SAMPLE ASSEMBLY

During the past 35 years of PPE technique development, many detection cells have been designed. They have been operated in both back and front configurations, making use of frequency or thickness scanning procedures. It is impossible to review all of these detection cells; therefore we will limit our presentation to several cells that were designed by our group, together with our co-workers. Alternative detection cells and set-ups can be found in Refs. [64–72].

One of the first detection cells to be developed, used by the authors for thermal inspection of liquid samples, is described in Fig. 9. It is based on the TWRC method.

The cell is based on two micrometer systems. One (with a precision of 5 μm) performs the sample thickness scan, by modifying the distance between the sensor and an irradiated (50 μm thick) Be foil; the second one (with a precision of 1 μm) ensures rigorous control of the thickness variation. The liquid sample fills the space between the sensor, the Be foil and a plastic ring, glued onto the sensor with silicone rubber. As stated above, precision in the thickness variation control offered by this cell is of about 1 μm. For high resolution measurements (required for example by molecular and/or isotopic association studies in liquid mixtures) this resolution may not be sufficient.[29, 30] As a result new detection cells, based on motors with nano-meter resolution, have been developed.

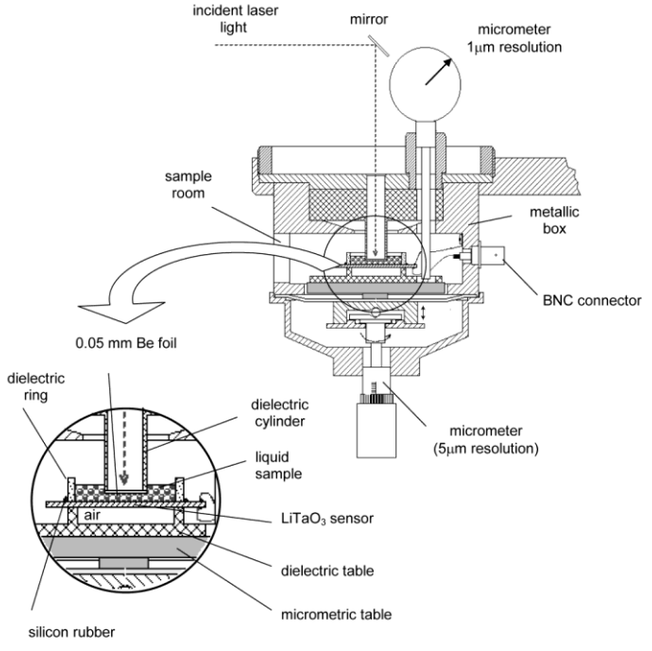

Fig. 9. Schematic view of a two-micrometric system used in back PPE configuration, TWRC method, for investigations of thermal parameters (thermal diffusivity) of liquids. [30] Reprinted from Dadarlat, D.; Neamtu, C. Acta Chim. Slov. 56 (1), 225-236, 2009; licensed under a Creative Commons Attribution (CC BY) license.

Figs. 10[30] and 11 present the evolution of the detection cells (nano-meter resolution) used in PPE calorimetry of liquids, based on the TWRC method.

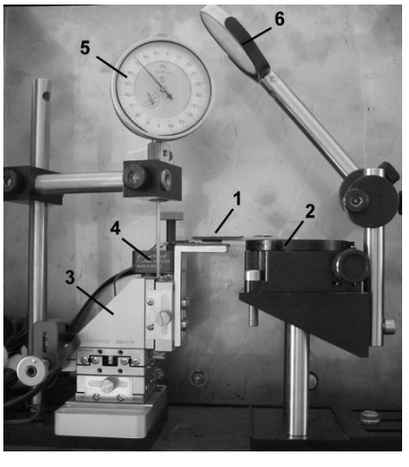

Fig. 10. Image of the detection cell used by for PPE calorimetry of liquids (TWRC method). 1 – PPE cell; 2 - rotating table; 3 – XYZ motion control system; 4 – nano-motor for vertical motion control; 5 – micrometer; 6 – mirror reflecting the incident laser radiation. [30] Reprinted from Dadarlat, D.; Neamtu, C. Acta Chim. Slov. 56 (1), 225-236, 2009; licensed under a Creative Commons Attribution (CC BY) license.

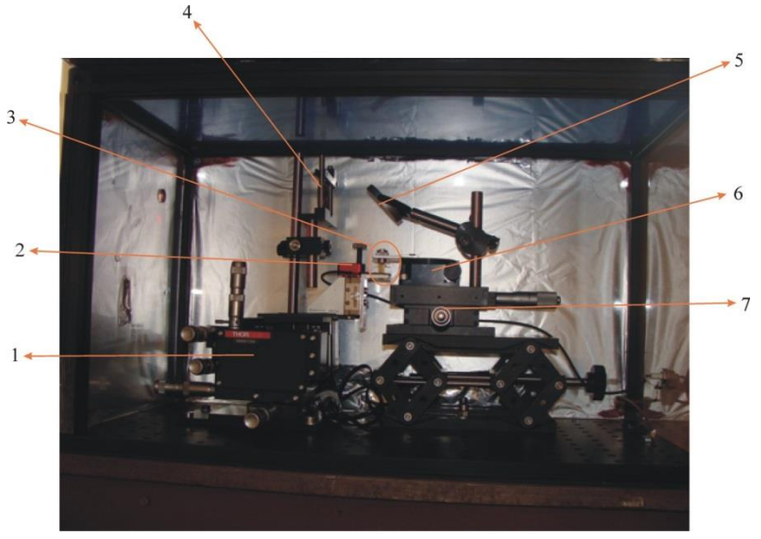

Fig.11. Image of the detection cell used for high accuracy PPE calorimetry of liquids (TWRC method). 1—nanoblock 6-axis manipulator, 2—nano-motor, 3—sensor-sample-backing assembly, 4—diaphragm, 5—adjustable mirror, 6—rotating table, 7—XYZ-translation stage).

The cells described above have been used for the PPE calorimetry of liquids at room temperature. They can be easily adapted for measurements on solid samples if the TWRC method is replaced by a frequency scanning procedure.

In the proceding section we will describe two concepts for detection cells used for temperature dependent PPE calorimetry.

The first cell is based on a cold-finger refrigerator system.[9] The cold-finger concept (Fig. 12) allows investigations at temperatures both below and above ambient conditions. The cell has two windows, for investigations in both BPPE and FPPE configurations. In principle, the copper bar transmits the temperature to the sample – one extremity of the bar can be cooled using liquid nitrogen, or heated electrically with a resistive coil. The role of the 0.1 mm thick steel cylinder is to keep the cell (except the copper bar) at room temperature. Depending on the operating temperature, one can make a vacuum inside the cell or introduce a dry atmosphere. The temperature of the sample is measured with a diode that is glued with silicon grease to the cold finger, in the vicinity of the sample.

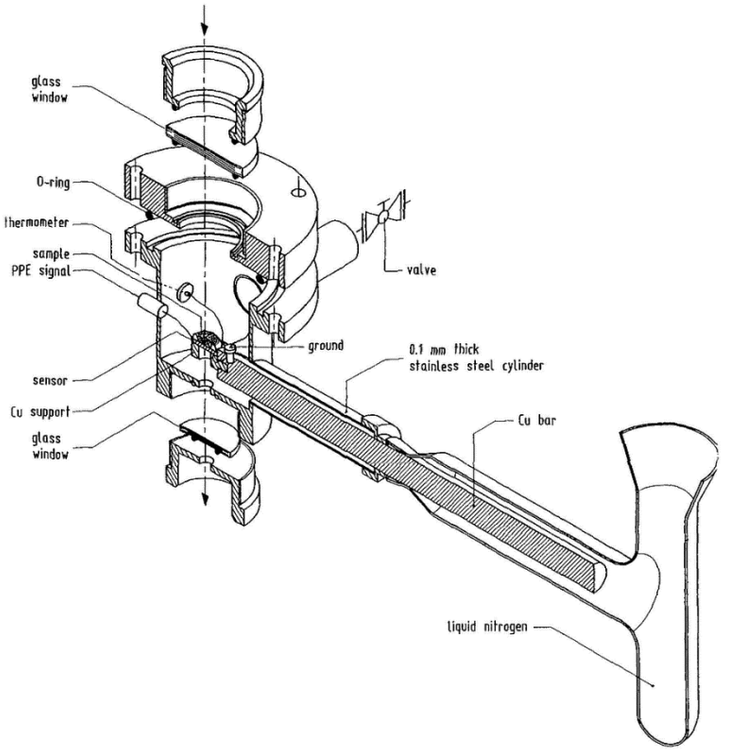

Fig.12. Cold finger refrigerator system.[9] Reproduced with permission from J. Am. Oil Chem. Soc. 72(3), 281 (1995). Copyright 1995 Springer Nature.

The second cell concept is based on a system that has Peltier elements for temperature scans. [63] The design of a PPE detection cell equipped with Peltier elements is presented in Fig. 13. One face of one of the two Peltier elements (electrically connected in parallel) is thermally connected to a thermostat (liquid flux from a thermostatic bath). The opposite face of the second Peltier element is in thermal contact with an inside-chamber that accommodates the sample-sensor assembly. Temperature feed-back is achieved with a thermistor placed close to the sensor. Computer-controlled temperature scans with positive/negative rates (heating/cooling) are possible.

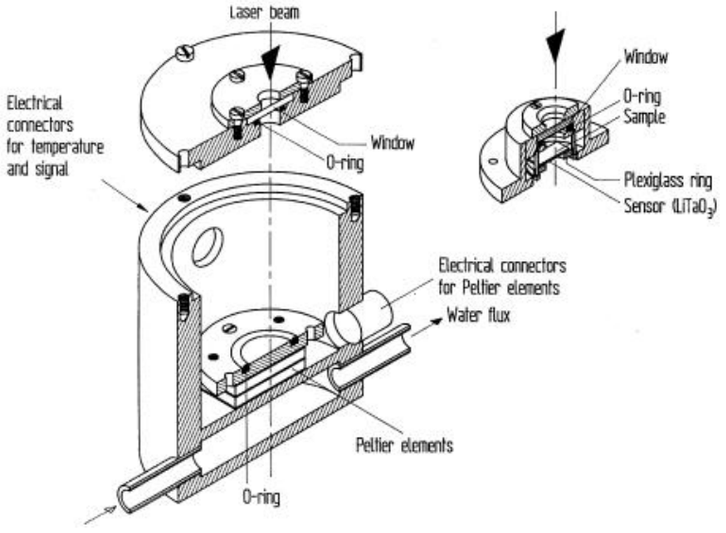

Fig.13. [9] PPE detection cell provided with Peltier elements. [9] Reproduced with permission from J. Am. Oil Chem. Soc. 72(3), 281 (1995). Copyright 1995 Springer Nature.

When investigating solid samples, the sensor-sample assembly is composed of the sensor and sample which is in thermal contact. A coupling fluid (silicone grease, ethylene glycol, water, etc.) is usually used at the sensor-sample interface (Fig. 14).

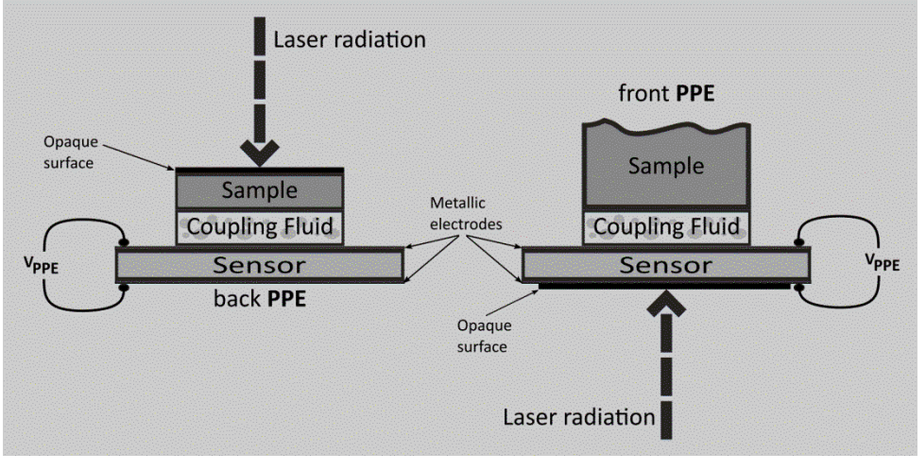

Fig.14. Sensor-sample assembly for solid samples.

The back detection configuration is used both for spectroscopic and calorimetric applications. It requires a flat sample of a reasonable thickness (10 μm – 500 μm). The front detection configuration is used only for calorimetric measurements and is dedicated to thermal effusivity measurements. This configuration requires only a flat surface in contact with the sensor and a geometrical thickness that can be considered "thermally thick" for the modulation frequencies used in the experiment.

When liquid samples are under investigation, the design of the detection cell is more complicated. Even if the contact between a liquid sample and a solid sensor is perfect and thus no coupling fluid is necessary, it is rather difficult to control exactly the liquid's (i.e., the sample) thickness. For thermal effusivity investigations, as in the case of solid samples, the

liquid is in a back position (front detection configuration) and knowledge of its thickness is not necessary. Therefore, liquid sample can fill the space inside a ring such as in Fig. 15. The only requirement in order to obtain the value of the thermal effusivity is that the sample is "thermally thick".

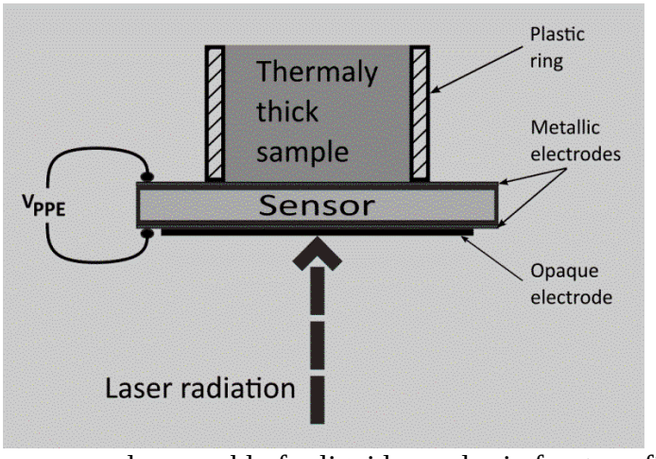

Fig.15. Sensor-sample assembly for liquid samples in front configuration.

For the analysis of solids using the back detection configuration, we can perform spectroscopic investigations or, just as in calorimetry, we can directly measure thermal diffusivity. However, for this purpose we need to know the precise sample thickness or its variation. This can be accomplished using a calibrated cell[74] or using the TWRC technique.

Fig. 16 displays a PPE detection cell for liquids that is used for spectroscopy in the "reflection mode". This mode, with on a calibrated cell, has been successfully applied to the analysis of the optical absorption bands of water in the near IR.[14]

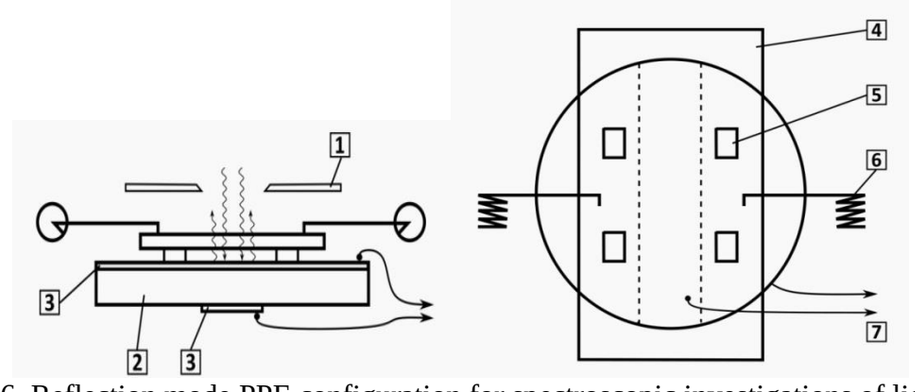

Fig.16. Reflection mode PPE configuration for spectroscopic investigations of liquids. (1- exit slit of the monochromator; 2- pyroelectric sensor; 3- reflecting gold electrodes; 4- glass window; 5-thin spacer; 6-joining spring; 7-output signal).

Fig. 9 presents the sensor-sample assembly in back detection configuration, for the TWRC method. As previously described, the distance between the sensor and the irradiated absorbent metallic layer (Be foil) is modified in a controlled way, by using a nano-motor. The thermal diffusivity of the liquid sample is obtained from the slope of the phase of the PPE signal as a function of sample thickness (Eq. 9). We will now describe a more complex sensor-sample assembly, used for the investigation of volatile liquids (Fig 17).

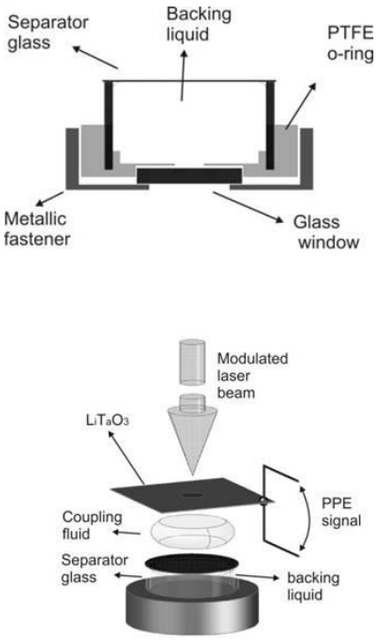

Fig.17. Sensor-sample assembly for the investigation of volatile liquids.

When volatile liquids are under study, we must somehow prevent their evaporation during the measurement process. One option is to encapsulate the liquid in a closed box fitted with two glass windows. A thin window (50 μm - 100 μm) acts as a separator between the liquid to be investigated (backing liquid in Fig. 16) and second liquid layer which acts as a coupling fluid between the separator and the pyroelectric sensor. Using a sensor-sample assembly such as this, one can directly measure the thermal effusivity of volatile liquids, however, for accurate results, the separator window must be considered as a layer in the theoretical assumption (it cannot be ignored).

In order to conduct experiments, one can combine the set-ups, detection cells and sensor/sample assemblies described above, in a convenient way, in order to measure both the thermal diffusivity and the effusivity of condensed matter samples.

4. APPLICATIONS

4.1.SPECTROSCOPIC APPLICATIONS

4.1.1. Spectroscopy of solids

As mentioned in the Introduction, the first PPE spectroscopic experiment was reported in 1984).[3] and described experiments on solid samples. Using the experimental set-up from

Fig. 4, the optical absorption bands of anodized Al (anodized in H_2SO_4 and $H_2C_2O_4$) in the near infrared (IR) (0.7 μm -20 μm) were detected. The experiment used a Globar source of radiation, a single prism monochromator and a TGS single crystal as pyroelectric sensor. This combination offered enough light intensity and spectral resolution to allow good quality measurements in the near (IR). No absolute values of absorption coefficients of the investigated materials were obtained, but the method proved to be useful in comparing the optical absorption of different non-transparent materials used as potential absorbent layers for IR detectors or laser energy meters (see Fig. 18).

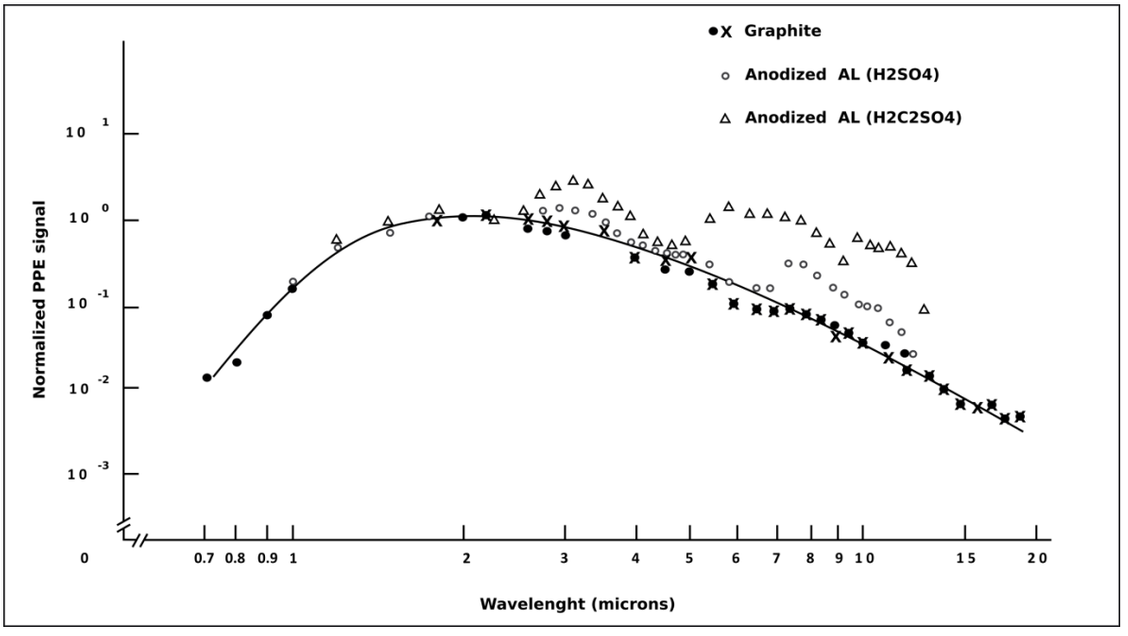

Fig. 18. Normalized PPE signals for graphite and anodized Al in the near IR.

Fig. 18 shows that graphite has a uniform optical absorption in the 0.7 μm – 20 μm spectral range. Al samples were anodized in H_2SO_4 and $H_2C_2SO_4$ and have selective optical absorption with strong absorption bands in the 2.5 μm – 4 μm and 6 μm – 15 μm spectral range. A more sophisticated study could be performed by using thermally-coupled and conventional PPE spectroscopy. The reader can find and example of such an experiment in Ref. [75], performed on hydrogen uranyl phosphate (HUP). The absorption bands found at about 1.25 μm, 1.5 μm and 2 μm can be correlated with higher protonic conductivity of HUP, suggesting polaronic effects on the conduction mechanism in this solid electrolyte.

4.1.2. *Spectroscopy of liquids*

When irradiating a liquid sample in contact with a pyroelectric sensor, the overall PPE signal is produced by the vector sum of two periodic heat sources. The first source, generated upon the absorption in the opaque pyroelectric, is proportional with the fraction of radiation transmitted through the sample. In this case, the radiation sensor acts as a radiation detector and produces a signal analogous to conventional transmission spectra. A second source arises due to radiation absorption within the partially transparent sample. For this signal component the pyroelectric sensor is a true thermal wave sensor, yielding a combined transmission-absorption spectrum. In the standard PPE configuration, the signal is often saturated due to the dominance

of the first heat source, especially for transparent samples. This is why it is useful to suppress it. The remaining PPE signal is expected to be richer in spectroscopic information. Experimentally, one can achieve this by using a pyroelectric sensor equipped with a highly reflected front electrode. This PPE configuration is termed "reflection mode pyroelectric" (RPPE) spectroscopy and it has been successfully used for the investigation of the optical properties of strongly absorbing liquids.[14]

Using the sensor-sample assembly in Fig. 16, the optical absorption bands of water in the near IR region have been detected.

In the near IR spectral region, H_2O and D_2O have three optical absorption bands at approximately 1.5 μm, 1.9 μm and 3 μm (H_2O) and 1.9 μm, 2.6 μm and 4 μm (D_2O). It can therefore be expected that the PPE spectrum in the 2 μm - 5 μm spectral range will be resolved with respect to peaks from 3 μm and 4 μm, respectively. We can therefore conclude that RPPE spectroscopy in the 2 μm -5 μm spectral range is able to detect the presence of both H_2O and D_2O in H_2O - D_2O mixtures. Two examples of results obtained by RPPE spectroscopic investigations on H_2O - D_2O mixtures are presented in Figs. 19 and 20.[76]

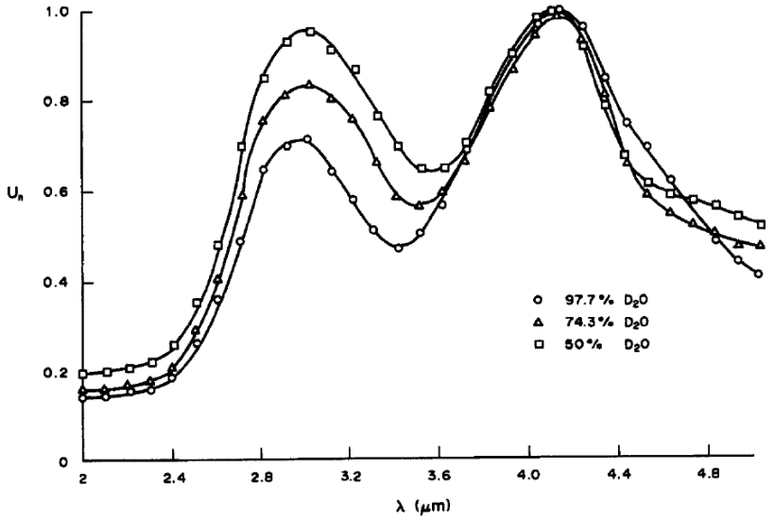

Fig.19. PPE amplitude, normalized at the value from 4 μm for H_2O - D_2O mixtures with a D_2O content larger than 50%.[76] Reproduced with permission from Infrared Phys. 33(6), 575 (1992). Copyright 1992 Elsevier.

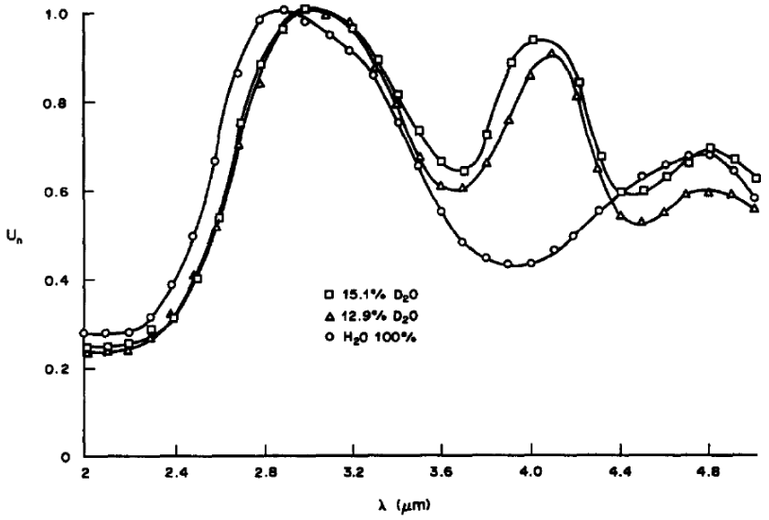

Fig. 20. PPE amplitude, normalized at a value from 3 μm for H_2O - D_2O mixtures with a D_2O content smaller than 50%. [76] Reproduced with permission from Infrared Phys. 33(6), 575 (1992). J Copyright 1992 Elsevier.

The amplitude of the absorption peaks is proportional to the component concentration, allowing a compositional analysis of these mixtures. In Ref. [76] several solutions allowing compositional analyses such as this are described.

4.2. CALORIMETRIC APPLICATIONS

4.2.1. Solid samples

When investigating solid samples, it is not easy to obtain accurate quantitative results, due to the influence of the coupling fluid placed between sample and sensor. PPE calorimetry is a contact technique and so coupling fluids, always necessary when investigating solids, lead to uncontrolled errors. Over the last two decades a lot of effort has been dedicated finding a way of eliminating the influence of the coupling fluid on results. Some researchers have tried to identify the most suitable coupling fluids and find mechanical methods that reduce their thickness.[38] Others have elaborated mathematical models in which they included the layer of coupling fluid in the detection sandwich (sample/coupling fluid/sensor).[39, 40] Another method to eliminate the influence of the coupling fluid was to use the aforementioned TWRC method.[20–31]

We can focus our attention on the front photopyroelectric (FPPE) configuration as in the past this was most commonly applied to obtain the thermal parameters of solid samples[9, 12, 16, 77, 78]. In most cases the FPPE detection cell contained three layers: air, a directly irradiated sensor and a solid semi-infinite sample. The value of thermal effusivity could be obtained by performing frequency scans of the amplitude or phase of the FPPE signal. Pittois et al.[79] designed for the first time a four layer FPPE cell, with a thermally thin solid sample and a semi-infinite backing material. With the restriction of "very good thermal conductor backing", they were able to derive both the thermal conductivity and the effusivity of the sample, by performing a frequency scan of the PPE signal over a large frequency range.

As mentioned above, Mandelis and co-workers proposed the TWRC method, as an alternative to frequency scanning procedures.[20, 28] It was demonstrated using a technique

which combined the FPPE configuration with the TWRC method. During the experiment the thickness of the coupling fluid was monitored and a solid material was used as a backing which lead to the direct measurement of the solid sample's thermal effusivity. In doing this the coupling fluid was no longer a disturbing factor and instead its properties could be used to obtain the value of the thermal effusivity.

The results of this application for a detection cell with ethylene glycol as a coupling fluid and different solids as backing materials are presented in Fig. 21: typical behaviors of the normalized phase of the FPPE signal can be seen.

As mentioned in the theoretical section, FPPE can be coupled with PTR in order to obtain calorimetric information. Using the experimental set-up from Fig. 7 together with the theoretical assumptions described previously (Eq. 34), one can simultaneously obtain values of the thermal effusivity samples (see Fig. 22)

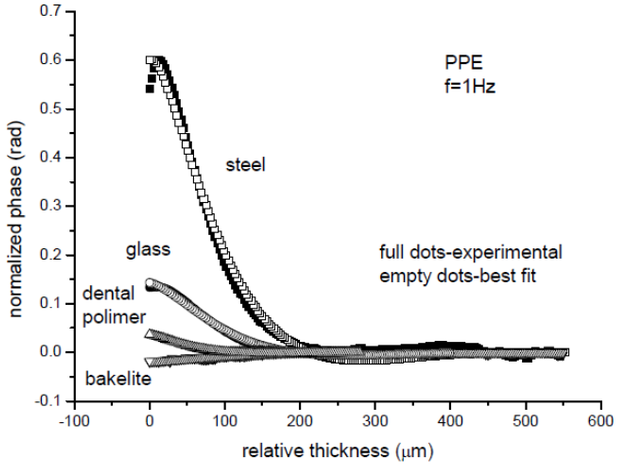

Fig. 21. Normalized PPE phase as a function of the relative thickness of the coupling fluid (ethylene glycol) for materials with different values of thermal effusivity.[80] Reproduced with permission from J. Therm. Anal. Calorim. 111(2), 1129 (2013). Copyright 2013 Springer.

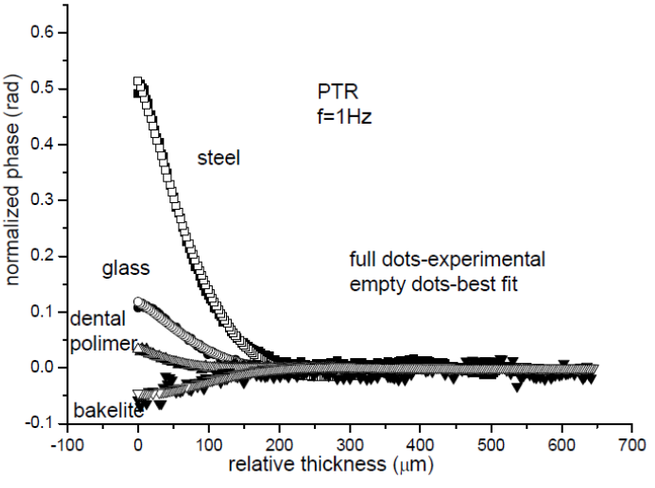

Fig. 22. Normalized PTR phase as a function of relative thickness of the coupling fluid (ethylene glycol) for materials with different values of thermal effusivity.[81] Reproduced with permission from J. Therm. Anal. Calorim. 118 (2), 623 (2014). Copyright 2014 Springer.

Fig. 23 illustrates some results obtained on dental polymers with different values of thermal effusivity. The results indicate that the thermal parameters for these dental materials are composition dependent. The values of the thermal effusivity of the dental polymers are important parameters in establishing their thermal biocompatibility.[80–82]

Results obtained at room temperature for the thermal effusivity of the solids under study are presented in Table 2, together with some available literature data.

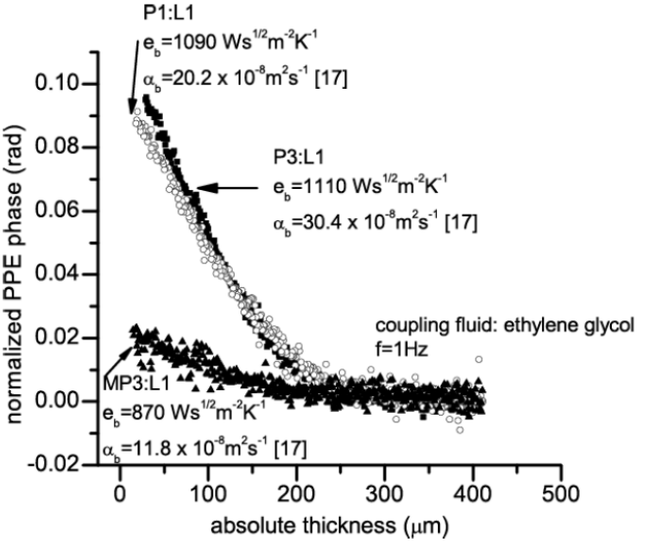

Fig. 23. Normalized PPE phase as a function of coupling fluid's thickness for some dental polymers with a different composition.[82] Reproduced with permission from J. Therm. Anal. Calorim. 119(1), 301 (2015). Copyright 2015 Springer.

Table 1. Room temperature values of thermal effusivity for the investigated solids, as obtained from PPE and PTR measurements, together with literature data.[86] Reproduced with permission from Proc. SPIE 8411, Advanced Topics in Optoelectronics, Microelectronics, and Nanotechnologies VI, 84110T (2012). Copyright 2015 SPIE.

Material	**Thermal effusivity ($Ws^{1/2}/m^2K$)**		
	PPE	**PTR**	**Literature**
Steel	6400	4900	6090 – 7187
Glass	1360	1280	1275 – 1600
Textolite	1040	1020	1000 – 1810
dental polymer	980	980	870 – 1110
Bakelite	760	680	681
Teflon	690	690	600 – 700
Propylene	520	490	-

The front photopyroelectric (FPPE) configuration, together with the TWRC method, has also been applied to the measurement of thermal diffusivity in thin solids. The methodology is based on an FPPE detection cell in which a thin solid layer is inserted between two layers of identical liquids—one layer in contact with the pyroelectric sensor acting as a coupling fluid and a second one acting as a backing layer.[87] The value of the thermal diffusivity is obtained as a result of a scan of the phase of the FPPE signal as a function of the coupling fluid's thickness (i.e., the TWRC method). The applicability of this method was demonstrated with experiments on solids of different thicknesses (50–200 μm) and values of thermal diffusivity (glass, steel, aluminum, copper)[87]. Fig. 24 displays the behavior of the normalized FPPE phase as a function of coupling fluid thickness, for a detection cell with 150 μm thick Al foil as a separator, and Table 2 summarises the results obtained for several foils. For the thicknesses reported in Table 2, it seems that the results are in rather good agreement with data obtained for bulk materials.

It should be noted that the very same method (same experimental measurement and same theoretical analysis) can be used to obtain the thermal effusivity of a thin solid layer, if its thermal diffusivity is known.

Table 2. Results obtained with the FPPE-TWRC method for the thermal diffusivity of the investigated samples, together with results reported in the literature. Column 3 contains the values of the thermal effusivity used in the fitting procedure. [87] Reproduced with permission from Meas. Sci. Technol. 21(10), 105701(2010). Copyright 2010 IOP Publishing.

Material	**Thickness (μm)**	**Th. effusivity ($Ws^{1/2}/m^2K$)**	**Th. dffusivity x 10^{-6} (m^2/s)**	
			Experiment	**Literature [88]**
Cu (alloy)	50	37000	61.4	32.9 – 117.3
Al (alloy)	150	25000	75.2	35.1 – 87.9
Steel	80	7200	3.3	3.5 – 19.7
Glass	200	1500	0.65	0.31 – 0.74

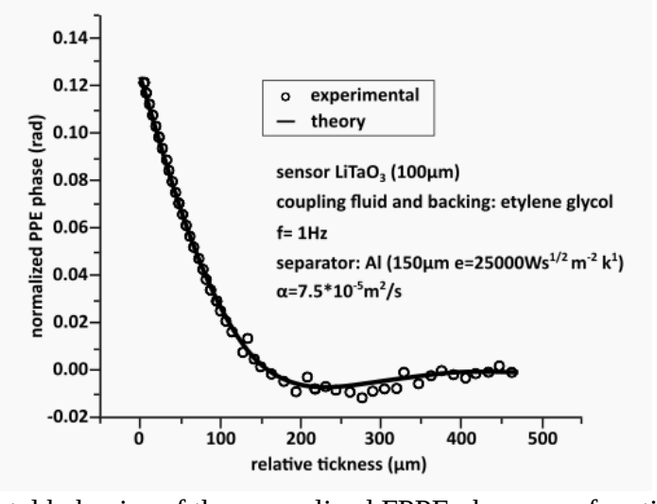

Fig. 24. The experimental behavior of the normalized FPPE phase as a function of coupling fluid's thickness, for a detection cell with the 150 μm thick Al foil as a separator. The best

theoretical fit is also displayed. [87] Reproduced with permission from Meas. Sci. Technol. 21(10), 105701(2010). Copyright 2010 IOP Publishing.

Another important application of the PPE technique is in the investigation of the thermal parameters of the pyroelectric sensors themselves. [89-93] For most applications concerning pyroelectric materials, knowledge of their thermal parameters is necessary because they are relevant for evaluating the figure of merit of an IR sensor[94] or a pyroelectric accelerator,[95] for instance. When used as a sensor in a PPE experiment, knowledge of these parameters is crucial, because all other measured properties depend of these values[96]. Moreover, it has been shown that these parameters have slightly different values as a function of the composition/purity of the pyroelectric material.[97]

In principle, in order to obtain the thermal parameters of a pyroelectric sensor, it must be inserted in a simple front PPE detection cell composed of three layers (air/pyroelectric sensor/substrate (backing) – see Fig.14). Performing a frequency scan of the FPPE signal, one can obtain the sensor's thermal parameters, based on information of both amplitude and the phase of the signal, provided that the thermal parameters of the backing material is known.[98, 99]

In the following paragraph we will describe the results obtained on a frequently used pyroelectric sensor $LiTaO_3$ single crystal.

The behavior of the normalized phase and amplitude of the PPE signal, as a function of frequency, obtained for a 510 µm thick $LiTaO_3$ single crystal is plotted in Fig.25.

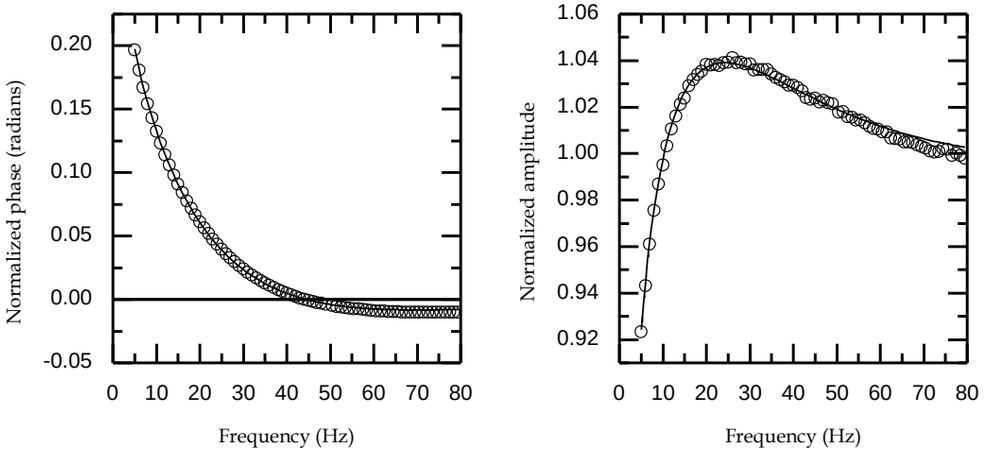

Fig. 25. Normalized signal's phase and amplitude obtained with a 510µm thick $LiTaO_3$ film and water as substrate (open circles: experimental data, solid line: best fit).[35] Reproduced from [Longuemart, S.; Sahraoui, A. H.; Dadarlat, D.; Delenclos, S.; Kolinsky, C.; Buisine, J. M. Study of Thermal Parameter Temperature Dependence of Pyroelectric Materials. Review of Scientific Instruments, 2003, 74 (1), 805–807. https://doi.org/10.1063/1.1516241], with the permission of AIP Publishing.

The phase and amplitude of the signal contain both information about the thermal diffusivity and effusivity of the ferroelectric material. From an analytical point of view, the phase goes to zero for a frequency f_0 which verifies the relationship:

$$\frac{L_p\sqrt{f_0}}{\sqrt{\alpha_p}} = \sqrt{\pi}\ . \qquad (35)$$

In this experiment, f_0 = 44.2 Hz which leads to a thermal diffusivity of 1.53 10^{-6} m^2/s for $LiTaO_3$. This value can be then used to extract R_{sp} ("*p*"- pyroelectric sensor, "s" – substrate) values and finally the thermal effusivity of $LiTaO_3$:

$$e_p = e_s\left(\frac{1-R_{sp}}{1+R_{sp}}\right) \tag{36}$$

As we know the thermal effusivity of the substrate, water (e_s =1580 $Ws^{1/2}/m^2K$), the average value of the calculated thermal effusivity is e_p = 3603 $Ws^{1/2}/m^2K$. A similar procedure can be adopted to extract the thermal parameters from the amplitude of the signal. The frequency f_1 corresponding to the maximum of the amplitude should verify the relationship:

$$\frac{L_p\sqrt{f_1}}{\sqrt{\alpha_p}} = \frac{3\sqrt{\pi}}{4} \tag{37}$$

Fig. 26 indicates that the amplitude has a maximum for a frequency f_1=25.3Hz, corresponding to a value of 1.56 10^{-6} m^2/s for the thermal diffusivity of $LiTaO_3$. From data of Fig.27, one finds e_p = 3821 $Ws^{1/2}/m^2K$.

Another way to obtain the sensor's thermal parameters is to combine the phase and the amplitude of the signal. In our model the normalized FPPE signal is given by the relationship:

$$V_n = 1-(1+R_{sp})\exp(-\sigma_p L_p)\,. \tag{38}$$

A plot of the modulus of the complex quantity (1-V_n) as a function of the square root of frequency should display a line with a slope equal to the value of the thermal diffusivity of the sample; an extrapolation of the curve to zero frequency leads to the value of the thermal effusivity. Such a calculation has been performed for the experimental data shown in Fig. 27 and the result is presented in Fig. 26.

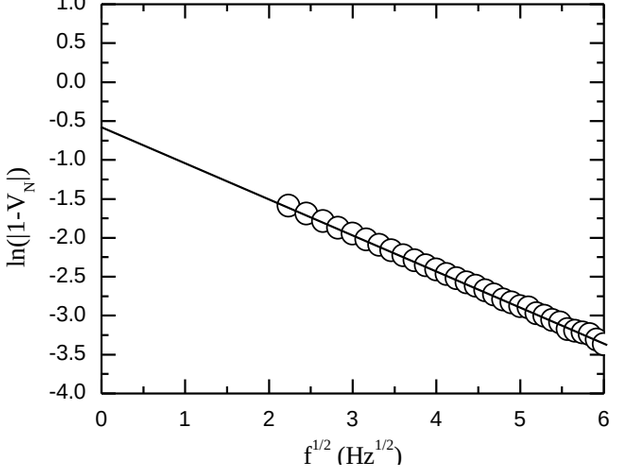

Fig. 26. Plot of the logarithm of |1-V_n| as a function of square root of frequency, for data presented in Fig. 26. [35] Reproduced from [Longuemart, S.; Sahraoui, A. H.; Dadarlat, D.; Delenclos, S.; Kolinsky, C.; Buisine, J. M. Study of Thermal Parameter Temperature Dependence of Pyroelectric Materials. Review of Scientific Instruments, 2003, 74 (1), 805–807. https://doi.org/10.1063/1.1516241], with the permission of AIP Publishing.

A linear fit of the data yields values of thermal parameters in agreement with previous calculated ones, as reported in Table 3.

Table 3. Comparison of values of thermal diffusivity and effusivity, obtained with various procedures, for a 510 µm thick $LiTaO_3$ single crystal.[35] Reproduced from [Longuemart, S.; Sahraoui, A. H.; Dadarlat, D.; Delenclos, S.; Kolinsky, C.; Buisine, J. M. Study of Thermal Parameter Temperature Dependence of Pyroelectric Materials. Review of Scientific Instruments, 2003, 74 (1), 805–807. https://doi.org/10.1063/1.1516241], with the permission of AIP Publishing.

	Thermal diffusivity ($x10^{-6}m^2/s$)	**Thermal effusivity ($Ws^{1/2}/m^2K$)**
Zero crossing (phase) Maximum (amplitude)	1.53 1.56	3821 3603
Combination of amplitude and phase (linear fit)	1.58	3886

The theoretical results we present here have been obtained without any hypothesis on the nature of the pyroelectric sensor. Whilst the experimental results were obtained on $LiTaO_3$ crystals, a similar procedure can be carried out for any type of pyroelectric material, such as PZT ceramics, polymer films (PVDF), etc.

One of the most challenging applications of PPE calorimetry is in the thermal characterization of porous solids. As mentioned above, for porous solids, any type of liquid or pasty coupling fluid penetrates into the sample and the obtained results are not accurate. The only alternative for PPE analysis of porous samples, is to replace the liquid/pasty coupling fluid between sensor and sample with a layer of air. A good example of this is in the analysis of building materials. For example, bricks collected from old buildings. It is well-known that accurate estimation of thermophysical parameters of building materials is critical for the evaluation and improvement of energy efficiency in the building sector and the development of new materials. In this respect, the science of building materials has mainly focused on maximizing or minimizing thermal conductivity, while thermal effusivity and diffusivity have received relatively limited attention, despite their importance when considering thermal energy exchange with the environment. The thermal regime of a building can be considered for a limited time interval as stationary, but during 24 hours, with significant temperature variations in a day/night cycle, the conditions are non-stationary. This is why correct and accurate measurement of thermal effusivity and diffusivity is very important in heat conduction studies for building materials.

Fig 27 displays the frequency behavior of the normalized FPPE phase for three bricks collected from old buildings (denoted samples 1 – 3), together with the best-fit performed with Eq. (19). [42]

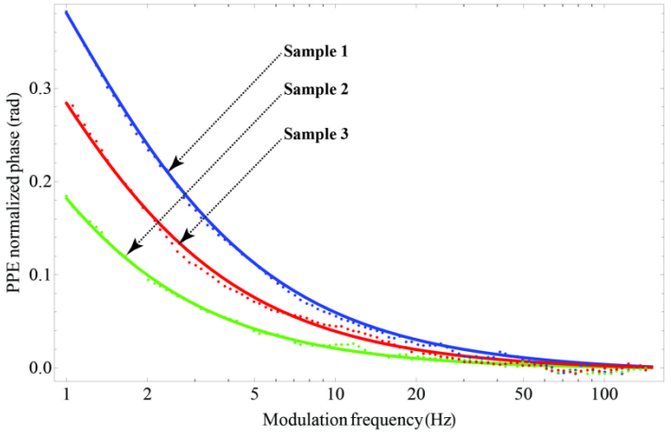

Fig. 27. The frequency behavior of the normalized FPPE phase for the investigated samples. The best fit performed with Eq. (19) is also presented. [42] Reproduced with permission from Thermochim. Acta. 702, 178943 (2021). Copyright 2021 Elsevier.

Table 4 shows the results obtained for the thermal effusivity of the investigated samples, together with the values obtained for the other two fitting parameters, h and L_a.

Table 4. The values of the fitting parameters for the investigated samples. [42] Reproduced with permission from Thermochim. Acta, 702, 178943 (2021). Copyright 2021 Elsevier.

Sample	**Thickness (μm)**	**Thermal effusivity ($Ws^{1/2}/m^2K)\cdot10^3$**	***H*** **(W/m^2K)**	***L_a*** **(μm)**
1	320	1.2± 0.1	42	17
2	770	0.9 ± 0.04	39	46
3	750	1 ± 0.07	40	26

Fig. 28 displays the behavior of the self-normalized PPE phase as a function of sqrt.(f) for the investigated samples (in the samples thermally thick regime) and Table 5 contains the values obtained for the thermal diffusivity, conductivity and volume specific heat.

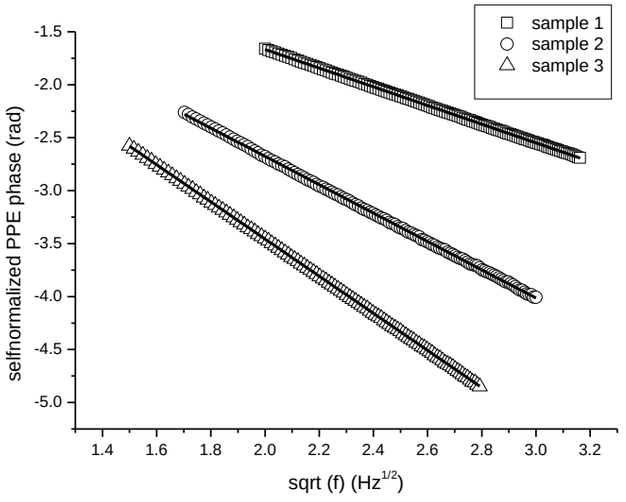

Fig. 28. Self-normalized PPE phase as a function of sqrt(f) for all investigated samples, in the samples thermally thick regime. [42] Reproduced with permission from Thermochim. Acta. 702, 178943 (2021). Copyright 2021 Elsevier.

Table 5. The values of thermal diffusivity *e*, thermal conductivity *k* and volume specific heat *C* obtained for the three samples of old bricks. [42] Reproduced with permission from Thermochim. Acta. 702, 178943 (2021). Copyright 2021 Elsevier.

Sample	**Thermal diffusivity ($10^6 m^2/s$)**	**Thermal conductivity (W/mK)**	**Volume specific heat ($10^{-6} J/m^3K$)**
1	0.41 ±0.02	0.75 ± 0.07	1.82± 0.12
2	1.04 ±0.03	0.91 ± 0.04	0.87± 0.04
3	0.56 ±0.02	0.70± 0.05	1.25± 0.08

The results obtained for the thermal parameters are in good agreement with those already reported for new and old bricks. This type of information becomes vital for many old buildings given their continued degradation over time.

4.2.2. Liquid (semi-liquid) samples

In this section we will select some applications of PPE calorimetry for liquids of great interest: liquid foodstuffs and magnetic nanofluids. These applications place emphasis on high resolution measurements for room temperature values of dynamic thermal parameters.

- ***(Semi)liquid foodstuffs***

Studies of the thermo-physical properties of foodstuffs represent an intensive research effort that has been carried out both in industry and academic institutions[99–105]. Once known and their behavior understood, such properties can be used to benefit industrial manufacturers by improving applications, as well as control the stability and the shelf life of the product. In this section we will present some applications in which accurate measurements of thermal parameters can lead to structural information.

The first example application is presented in Fig. 29. The thermal diffusivity of several commercially available margarines was measured in front configuration, using the thickness-scan method of the phase of the PPE signal. The value of the thermal diffusivity was obtained from the slope of the graph. A clear correlation between the values of thermal diffusivity and fat content was found.

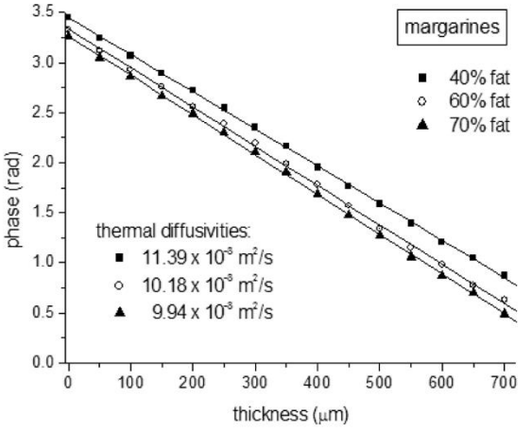

Fig. 29. Typical thickness scan of the phase of the PPE signal for three types of margarines with different fat content. [73] Reproduced from D. Dadarlat, and C. Neamtu, Recent Development of Photopyroelectric Calorimetry of Liquids**,** in Thermal wave physics and related photothermal techniques: Basic principles and recent developments, Ernesto Morales Marin (Ed.), Kerala, India, 65 (2009). All rights reserved.

When accurate measurements are performed, thermal diffusivity can be correlated with the fatty acid composition of various types of fats. An example is presented in Fig. 30. for vegetable oils.

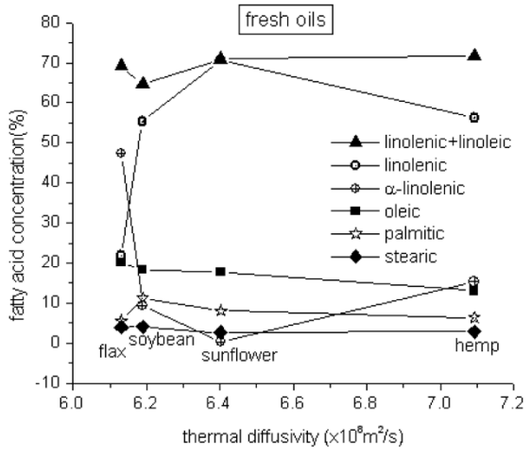

Fig. 30. Thermal diffusivity vs. concentration of stearic, palmitic, oleic, α-linolenic and linoleic fatty acids, for the investigated fresh oils. [30] Reprinted from Dadarlat, D.; Neamtu, C.

Acta Chim Slov, 56 (1), 225-236, 2009; licensed under a Creative Commons Attribution (CC BY) license.

A clear correlation can be observed between the values of the thermal diffusivity and the percentage of total (linoleic + linolenic) unsaturated fatty acids; the total amount of fatty acids slightly decreases with decreasing thermal diffusivity.

- ***Magnetic nanofluids***

Ferrofluids represent a special category of smart nanomaterials, consisting of stable dispersions of magnetic nanoparticles in different liquid carriers. Whilst magnetic properties of magnetic nanofluids are the subject of intensive study, there are far fewer data in literature concerning their thermal properties. Normally, thermal properties of magnetic nanofluids must depend on the composition of the nanofluid: the type of nanoparticles, the surfactant and carrier fluid, the concentration, nanoparticle size, etc. Furthermore, values of the static and dynamic thermal parameters and their temperature behavior are correlated with structural changes and/or the dynamics of various processes occurring inside the nanofluid.

Conversely, the little calorimetric data available indicate sometimes drastic changes in the thermal conductivity of nanofluids as a function of nanoparticle size. This is the case for Cu nanoparticles and carbon nanotubes immersed in ethylene glycol, for example[106, 107].
Due to the correlation between thermal parameters and the compositional parameters of nanofluids, PPE calorimetric studies of magnetic nanofluids can provide a lot of information.[108–110]

In the next section we will present results (obtained with the PPE technique) describing the correlation between the thermal and compositional parameters of nanofluids.

-Correlations in thermal diffusivity – type of carrier fluid and nanoparticles concentration

Fig. 31 presents a thickness scan of thermal diffusivity, obtained for nanofluids based on Fe_3O_4 nanoparticles stabilized by a double layer of oleic acid, but with different carrier fluids: water and decahydronaphtalene (DHNA).

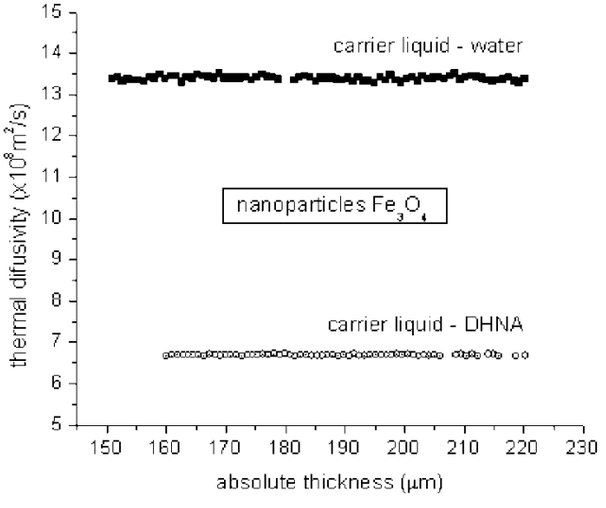

Fig. 31. Typical thickness scans of the thermal diffusivity, in the thermally thick regime for the sample, for nanofluids with Fe_3O_4 nanoparticles, stabilized with double layer of oleic acid

in different carrier liquids: water and DHNA. [30] Reprinted from Dadarlat, D.; Neamtu, C. Acta Chim. Slov. 56 (1), 225-236, 2009; licensed under a Creative Commons Attribution (CC BY) license.

Fig. 32 displays thickness scans of thermal diffusivity for water-based nanofluids with different concentrations of $CoFe_2O_4$ nanoparticles.

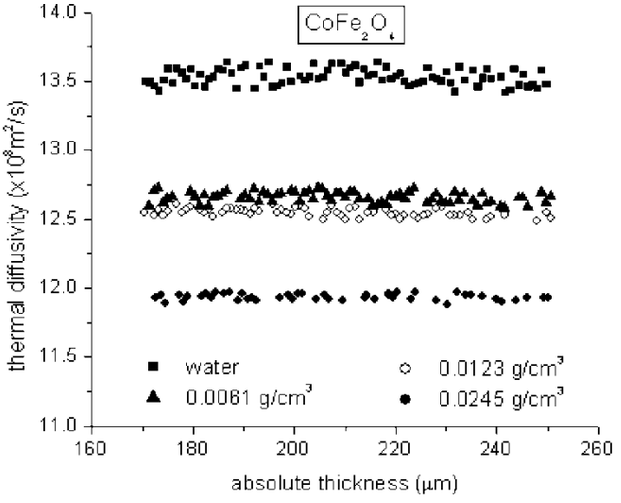

Fig. 32. Results of thickness scans obtained for the thermal diffusivity of water-based nanofluids with $CoFe_2O_4$ nanoparticles at different concentrations. [30] Reprinted from Dadarlat, D.; Neamtu, C. Acta Chim. Slov. 56 (1), 225-236, 2009; licensed under a Creative Commons Attribution (CC BY) license.

Figs. 31 and 32 indicate that thermal diffusivity is a sensitive to changes of other important nanofluid parameters such as the type of carrier liquid and the concentration of nanoparticles.

- Correlations in thermal effusivity – type of carrier fluid and nanoparticles concentration

In the next example, thermal effusivity was measured in the front configuration by making use of a frequency scan (i.e., based on the method proposed in Ref. [33]).

Figs. 33 and 34 present the results obtained for thermal effusivity. The same nanofluid samples were used for these experiments.

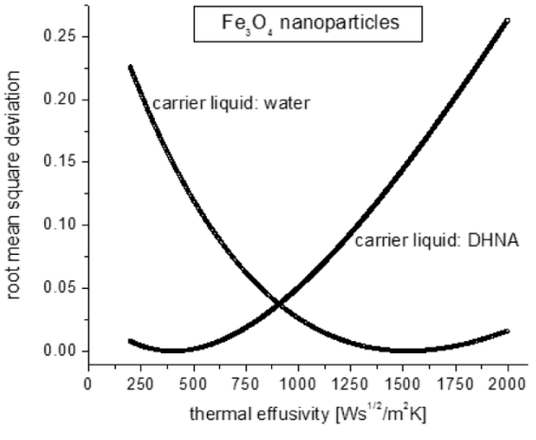

Fig. 33. Root mean square deviation of the fit performed on the experimental data (PPE phase as a function of chopping frequency), with the thermal effusivity of the sample as a fitting parameter. The minimum of the curve indicates the correct value of the thermal effusivity. Sample: nanofluid with Fe_3O_4 nanoparticles and different liquid carrier (water and DHNA).[30] Reprinted from Dadarlat, D.; Neamtu, C. Acta Chim. Slov. 56(1), 225-236, 2009; licensed under a Creative Commons Attribution (CC BY) license.

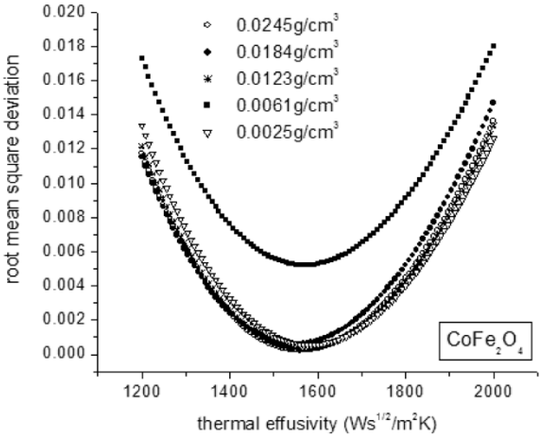

Fig. 34. Root mean square deviation of the fit performed on experimental data (PPE phase as a function of chopping frequency), with the thermal effusivity of the sample as a fitting parameter. The minimum of the curve indicates the correct value of the thermal effusivity. Sample: water-based nanofluid with $CoFe_2O_4$ nanoparticles.[109] Reproduced with permission from Int. J. Thermophys. 36(9), 2441 (2015). Copyright 2015 Springer Science+Business Media publishing.

As is apparent on inspection on Figs. 33 and 34, thermal effusivity also depends on the main parameters of the nanofluid, but it is less sensitive than the thermal diffusivity. The changes in thermal effusivity as a function of liquid carrier are clearly detected, but the changes as a function of nanoparticle type and concentration lie somewhere within the precision of the measurement at approximately ±1%.

-Influence of the type of surfactant on thermal parameters

In order to obtain this information, five types of magnetic nanofluids, based on Fe_3O_4 nanoparticles with water as a carrier liquid, were investigated using both PPE detection configurations (back and front) together with the TWRC technique as a scanning procedure. The type of surfactant varied between the nanofluids including: double layers of Lauric (LA-LA), Oleic (OA-OA) and Miristic (MA-MA) acids and also double layers of Lauric-Miristic (LA-MA) and Palmitic-Oleic (PA-OA) fatty acids. In both detection configurations, the information was contained in the phase of the PPE signal. The thermal diffusivity of nanofluids was obtained in the BPPE configuration, from the scan of the phase of the signal as a function of the liquid thickness. Using the same scanning procedure in the FPPE configuration, the thermal effusivity was measured directly.

Typical plots of the relative phase of the BPPE signal at room temperature as a function of nanofluid thickness are shown for the linear region of the graph in Fig. 35.[108] Room temperature thermal diffusivity can be calculated from the slope of the curves (Eq. 7).

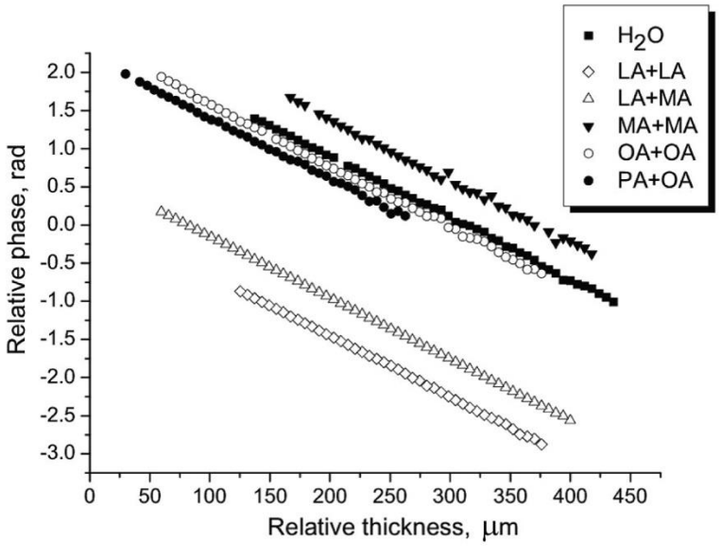

Fig. 35. Relative BPPE phase as a function of relative thickness for the investigated magnetic nanofluids. The results for water are presented for comparison. [108] Springer Science+Business Media publishing. Reproduced with permission from Int. J. Thermophys. 2014, 35(11), 2032 (2014). Copyright 2014 Springer Science+Business Media publishing.

Having obtained the values of thermal diffusivity, the thermal effusivity can be obtained in front detection configuration using the method proposed in Ref. [108] . Fig. 36 presents the behavior of the phase of the FPPE signal as a function of the relative thickness of the coupling fluid.

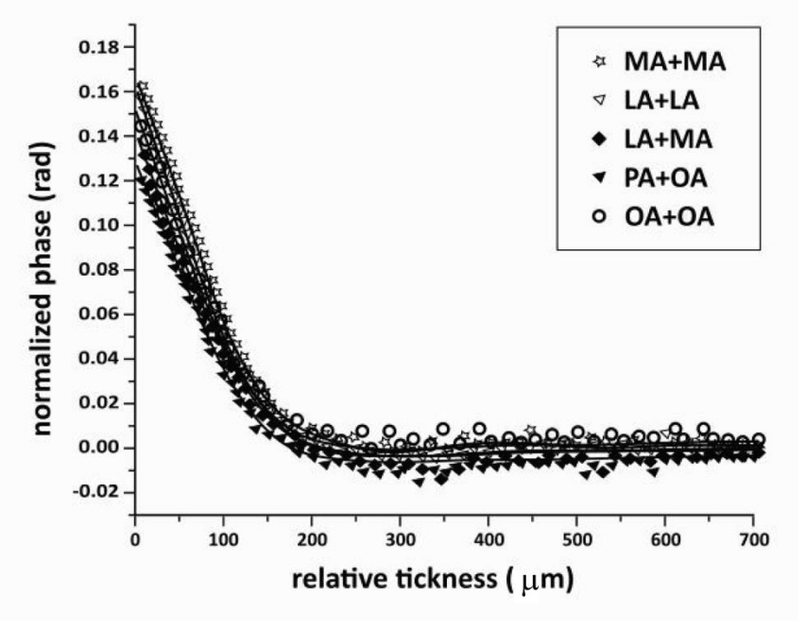

Fig. 36. Normalized phase of the PPE signal at f=1Hz, in the front configuration, as a function of relative thickness of the coupling fluid (ethylene glycol). [108] Reproduced with permission from Int. J. Thermophys. 35(11), 2032 (2014). Copyright 2014 Springer Science+Business Media publishing.

The results obtained for the values of the thermal diffusivity and effusivity are listed in Table 6. The table also contains the values of the remaining thermal parameters: thermal conductivity and volume specific heat (obtained from calculation).

Table 6. Values of the static and dynamic thermal parameters of the nanofluids based on Fe_3O_4 nanoparticles with water as carrier liquid and a variety of surfactants. [108] Reproduced with permission from Int. J. Thermophys. 35(11), 2032 (2014). Copyright 2014 Springer Science+Business Media publishing.

Type of surfactant	**Th. Diffusivity (10^{-8} m^2/s)**	**Th. Effusivity ($Ws^{1/2}/m^2K$)**	**Th. Conductivity (W/mK)**	**Vol. sp. Heat (10^4 J/m^3K)**
H_2O	14.54	1560	0.60	408.1
LA+LA	14.76	1600	0.61	413.2
LA+MA	14.54	1530	0.58	398.9
PA+OA	14.76	1790	0.69	465.6
OA+OA	14.47	1720	0.66	451.5
MA+MA	14.79	1700	0.65	441.6

In conclusion, it was found that different types of surfactants changed the thermal effusivity for the nanofluids under study by up to approximately 16%. The value of thermal diffusivity is practically unmodified by the type of surfactant.

-Influence of type and size of nanoparticles on thermal parameters

For this investigation two types of carrier liquids (transformer oil and polypropylene glycol) were combined with two types of iron based magnetic nanoparticles (Fe_3O_4 and $MnFe_2O_4$). Different sizes (10 nm – 80 nm) and shapes (spherical, octahedral or cubic) of nanoparticles were obtained, depending on the oleic acid/oleylamine molar ratio.[110]

The results obtained for the values of the thermal diffusivity for the various combinations of polypropylene glycol/ transformer oil and $MnFe_2O_4$/Fe_3O_4 are displayed in Fig. 37.

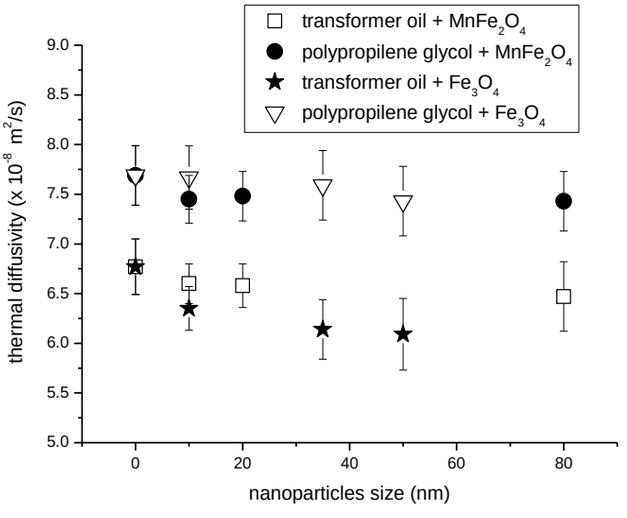

Fig. 37. The results obtained for the thermal diffusivity of the investigated magnetic nanofluids as a function of nanoparticle size. [110] Reproduced with permission from Int. J. Thermophys. 38(6), 86 (2017). Copyright 2017 Springer Science+Business Media publishing.

The corresponding results obtained for the thermal effusivity for all combinations of polypropylene glycol/ transformer oil and $MnFe_2O_4$/Fe_3O_4 are displayed in Fig. 38.

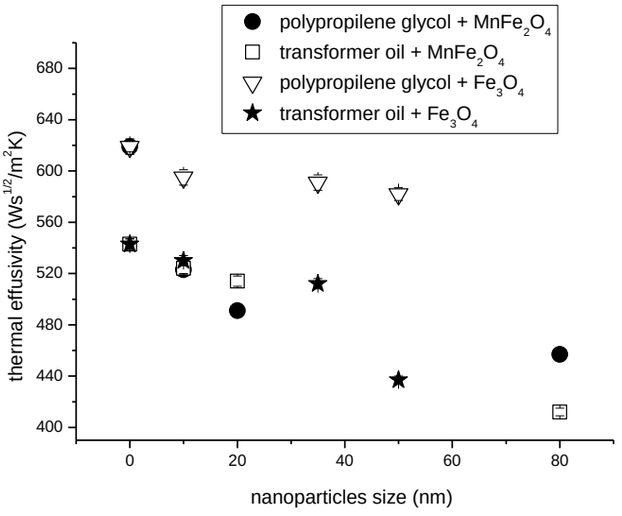

Fig. 38. The results obtained for the thermal effusivity of the investigated magnetic nanofluids as a function of nanoparticle size. [110] Reproduced with permission from Int. J. Thermophys. 38(6), 86 (2017). Copyright 2017 Springer Science+Business Media publishing.

The results obtained by the PPE technique indicate that the presence of the nanoparticles decreases the value of the thermal parameters of pure carrier liquids and both thermal diffusivity and effusivity decrease with increasing nanoparticle size, independent of the carrier liquid. The influence of nanoparticle size is more pronounced for the thermal effusivity (relative change 24%) compared with the thermal diffusivity (relative change 7%).

4.3. APPLICATIONS TARGETING STUDIES OF PHYSICAL AND CHEMICAL PROCESSES

As mentioned in the **Introduction**, optical and thermal properties are important parameters in many physical/chemical processes. The PPE method therefore provides a suitable technique to investigate processes associated with compositional changes (molecular associations, food adulteration) and structural/magnetic/electric changes induced by temperature variation (phase transitions). In this section we present examples of several such applications.

4.3.1. Molecular associations in binary (isotopic) liquid mixtures.

Assume that we mix two liquids. There are two possibilities: the liquids can mix in a non-associative way (non-interacting liquids) or they are able to form molecular associations.

If one intends to investigate the associative character of a liquid mixture, they must study the behavior of the thermal parameters of the mixture as a function of composition. For non-associative liquids the additivity law is respected and, as a consequence, a linear dependence of thermal parameters as a function of % mass composition is found. If molecular associations are present, thermal parameters depart from the linear additive law.

As an example, the excess value curves for the thermal diffusivity for various water-solvent mixtures as a function of solvent concentration are displayed in Fig. 39. Thermal diffusivity was measured in the back configuration using the sample thickness scan method, as proposed in Ref. [105]. The excess value curves presented in Fig. 39 demonstrate the associative character of water-based binary liquid mixtures.[23, 30, 73]

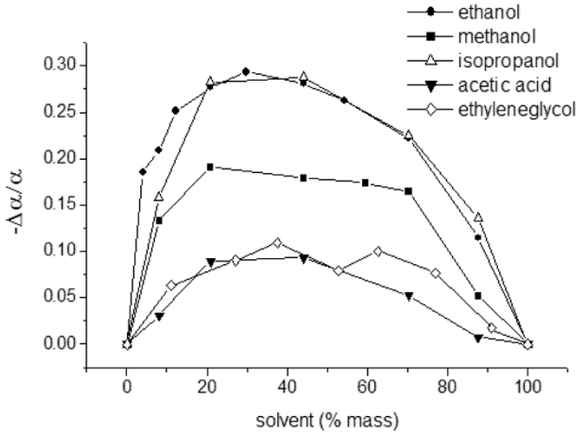

Fig. 39. Excess value curves for thermal diffusivity (plotted for convenience with negative sign) for various water-solvent mixtures as a function of solvent concentration. [73] Reproduced from D. Dadarlat, and C. Neamtu, Recent Development of Photopyroelectric Calorimetry of Liquids**,** in Thermal wave physics and related photothermal techniques: Basic principles and recent developments, Ernesto Morales Marin (Ed.), Kerala, India, 65 (2009). All rights reserved.

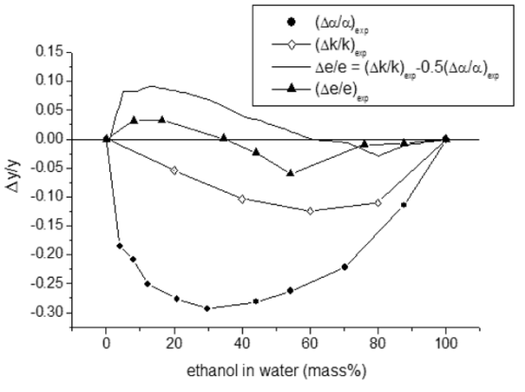

Fig. 40. Excess value curves for all thermal parameters for various water-ethanol mixtures, measured and as obtained from calculations. [73] Reproduced from D. Dadarlat, and C. Neamtu, Recent Development of Photopyroelectric Calorimetry of Liquids**,** in Thermal wave physics and related photothermal techniques: Basic principles and recent developments, Ernesto Morales Marin (Ed.), Kerala, India, 65 (2009). All rights reserved.

Fig. 40 presents the composition behavior of all thermal parameters for various water-ethanol mixtures. It is clear that the sensitivity to molecular associations in liquid mixtures is higher for the thermal diffusivity compared to other thermal parameters. Some deviations are observed for thermal effusivity, though they are not specific. Small deviations from additivity may occasionally be observed for non-associative mixing.[23]

When considering the applications presented above, PPE calorimetry applied to isotopic liquid mixtures represents a challenge; small deviations from linearity are expected for thermal parameters as a function of composition. Let us consider the case of mixtures of H_2O-D_2O and two isotopic dimethylsulfoxide species, C_2H_6OS and C_2D_6OS (denoted by DMSO(6H) and DMSO(6D)). In this example, the thermal diffusivity was measured in the back configuration using the sample thickness scan method[105], and the thermal effusivity was measured in the front configuration with a frequency scan of the phase of the signal.[87]

The obtained relative deviations from additivity for the thermal diffusivity and effusivity for H_2O-D_2O, DMSO(6H)-DMSO(6D) and H_2O-DMSO(6H) are presented in Figs. 41 and 42, respectively

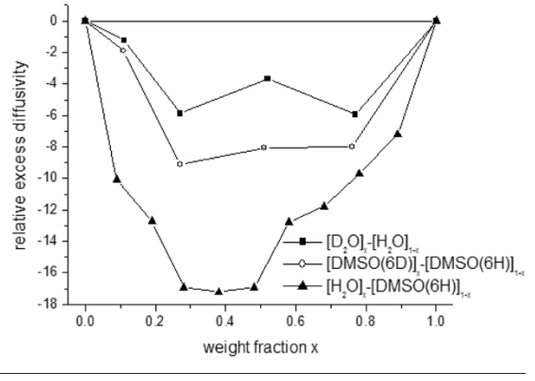

Fig. 41. Relative deviations from additivity of the thermal diffusivity for H_2O-D_2O and DMSO(6H)-DMSO(6D), together with a mixture (H_2O-DMSO(6H)) known for its "aggressivity" in forming molecular associations. [30] Reprinted from Dadarlat, D.; Neamtu, C. Acta Chim. Slov. 56 (1), 225-236, 2009; licensed under a Creative Commons Attribution (CC BY) license.

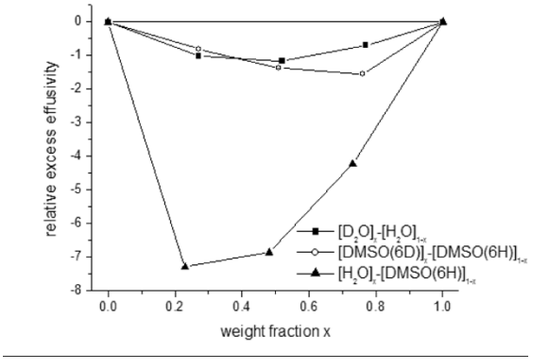

Fig. 42. Relative deviations from additivity of the thermal effusivity for H_2O-D_2O and DMSO(6H)-DMSO(6D), together with a mixture (H_2O-DMSO(6H)) known for its "aggressivity" in forming molecular associations. [30] Reprinted from Dadarlat, D.; Neamtu, C. Acta Chim. Slov. 56 (1), 225-236, 2009; licensed under a Creative Commons Attribution (CC BY) license.

The maximum relative deviation from additivity of the thermal diffusivity for H_2O-DMSO(6H) mixtures is about -18% and indicates association processes taking place in this system. In fact, DMSO is well known for its hygroscopic character. Conversely, the maximum relative deviations from additivity of the thermal diffusivity for H_2O-D_2O and DMSO(6H)-DMSO(6D) are about -4% and -8%, respectively. This can only be explained by an isotopic effect because, from a chemical point of view, H_2O and D_2O, and DMSO(6H) and DMSO(6D) molecules, are almost equivalent.

4.3.2. Vegetable oil adulteration

In order to study such a process, accurate PPE investigation with the TWRC method must be combined with another conventional technique for compositional analysis (gas chromatography (GC), for example). In Figs. 43 and 44 two methods were combined in order to detect adulteration of flax oil with sunflower oil.[95] The behavior of the thermal diffusivity as a function of sample thickness for flax-sunflower oil mixtures is presented in Fig. 43. Fig. 44 describes the correlation of thermal diffusivity with the content of relevant fatty acids (stearic, α-linolenic and the total amount of polyunsaturated fatty acids (PUFAs))

The plots indicate that the thermal diffusivity of the mixtures ranges from 8.07×10^8 m^2/s (pure sunflower oil) to 10.03×10^8 m^2/s (pure flax oil) and is directly correlated with the total amount of the polyunsaturated fatty acids in oils.[111]

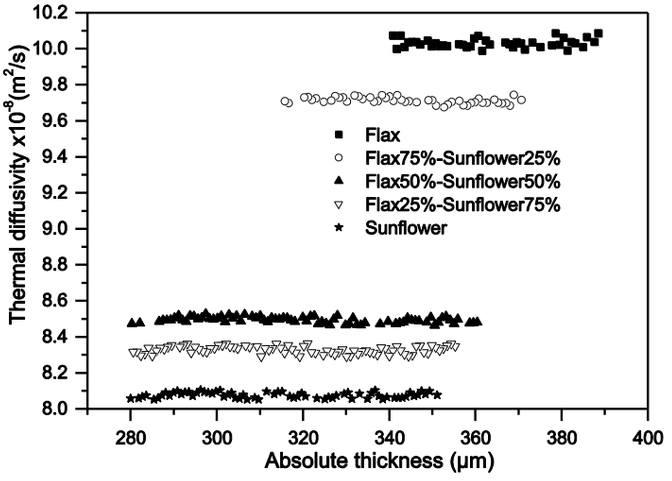

Fig.43. Typical thickness scans of the thermal diffusivity, for the flax-sunflower oil mixtures. [111] Reproduced with permission from Food Biophys. 4(3), 147 (2009). Copyright 2009 Springer Nature Publishing.

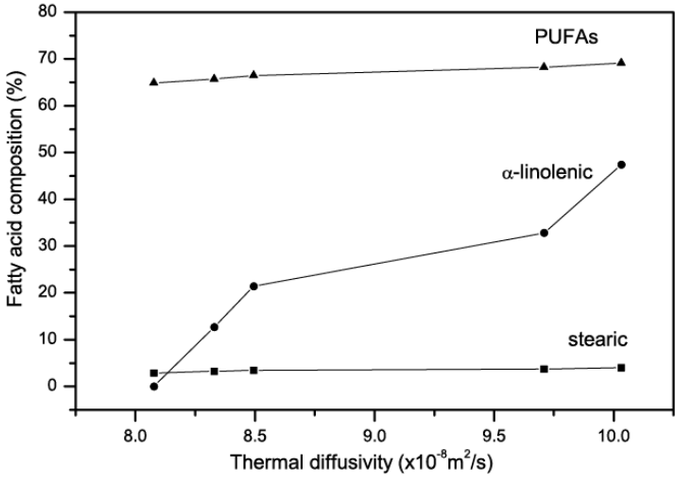

Fig. 44. Correlation of thermal diffusivity with the content of relevant fatty acids. [111] Reproduced with permission from Food Biophys. 4(3), 147 (2009). Copyright 2009 Springer Nature Publishing.

The correlation between the PPE signal and the composition of unadulterated and adulterated vegetable oils confirms the data obtained previously on fresh and spoiled vegetable oils[112] and suggests that thermal diffusivity may be a suitable parameter to determine the quality of oils and their early spoilage and adulteration. Another parameter that can be used detect oil adulteration is the freezing point, which can also be detected by the PPE method (see the section dedicated to phase transitions).

4.3.3. Phase transitions

A phase transition is a phenomenon associated with a break in the system's symmetry[45]. Usually, at the transition temperature, the system passes from an ordered to a disordered phase. The transition is always associated with fluctuations of the order parameter. As a consequence of these fluctuations, the derivatives of the thermodynamic potential present

anomalies in the critical region. If the first derivatives of the thermodynamic potential are discontinuous, the phase transition is of 1st order. If the first derivatives of the thermodynamic potential are continuous and the second derivatives are discontinuous, the phase transition is of 2nd order. The most common 1st order phase transitions are associated with melting, vaporization, etc. The most common 2nd order phase transitions are magnetic and ferro-paraelectric. If one intends to detect and study a phase transition, they must be able to measure a quantity (parameter) that presents an anomaly at the critical point. These parameters can be specific for different classes of materials (magnetization for magnets, polarization for ferroelectrics, etc.), but they can also characterize all types of materials; among this last type of parameters are the thermal parameters. As calorimetry is able to directly measure thermal parameters it is particularly suitable for phase transition studies. As presented in the theoretical section, the amplitude and phase of the complex PPE signal depend on two (or sometimes one) thermal parameters related to the sample. Theory dictates that the PPE technique is suitable to detect both first and second order phase transitions, by measuring critical anomalies of thermal parameters.

One of the most important factors in making high-temperature-resolution measurements of thermal parameters in the critical region of a phase transition is that the thermal gradients in the sample under investigation must be as small as possible. Often, at a phase transition the thermal parameters have a strong temperature dependence when approaching the critical temperature. Thermal gradients tend to smooth-out this temperature dependence and, sometimes, the phase transition is difficult to detect. To avoid this effect, it is important to keep the sample in quasi-thermal equilibrium. In most cases measuring techniques are based on detection of a rise in sample temperature as a response to a heat input but are themselves additional sources of temperature gradients. This is especially true of ac techniques. Accordingly, techniques that involving periodic sample heating are preferred, and the PPE technique is among them.

Over time, the PPE technique became increasingly applied to detect second[11, 74, 98, 114–121] or first[2, 9, 122–124] order phase transitions. For second order phase transitions PPE results were used to calculate the critical exponents of thermal parameters and to validate existing theories. Due to the fact that the PPE technique uses thermal parameters for phase transition investigations, a wide range of condensed matter specimens have been investigated: ordinary liquids and liquid mixtures; liquid crystals; liquid, pasty or solid foodstuffs; ferroelectric, thermoelectric and magnetic materials; high T_c superconductors; plastics and more.

The PPE study of phase transitions essentially developed over the last few decades due to the suitability of this technique towards this type of investigation. For readers who are interested in this topic, we recommend Ref. [74] and references therein.

From an experimental point of view, in order to study a phase transition by PPE, one has to use a detection cell that allows a sample temperature scan (see Figs. 12, 13). Both back and front PPE configurations can be used in order to detect a phase transition.[9] The critical temperature can be easily detected through the critical anomalies of the amplitude and phase of the PPE signal. However, if the critical behavior of the thermal parameters is the target of the investigation, things become more complex. One has to use the back detection configuration together with the information contained in both the amplitude and phase of the signal[11], or use a combination of back/front detection.[41] Additionally, calibration of the measurement at the given temperature (usually room temperature) is necessary.

In the following we will select only specific applications that concern both first and second order phase transitions, developed by the authors and coworkers.

4.3.3(a). First order phase transitions

As an example of PPE detection of first order phase transitions, we present results obtained on four samples of commercial Royal Jelly (RJ), provided by different producers.[125] Measurements were conducted in the front PPE configuration, in the -15˚C - 5˚C temperature range. Figs. 45 and 46 display the amplitude of the PPE signal as a function of temperature for the samples, in a temperature range that includes the transition (solid/liquid) point (heating-cooling cycles).

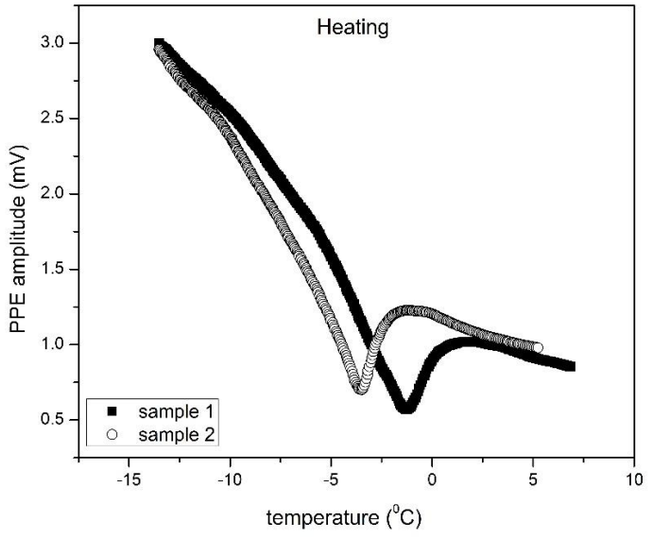

Fig. 45. PPE amplitude as a function of temperature for the RJ samples under investigation, in a temperature range including the melting point.

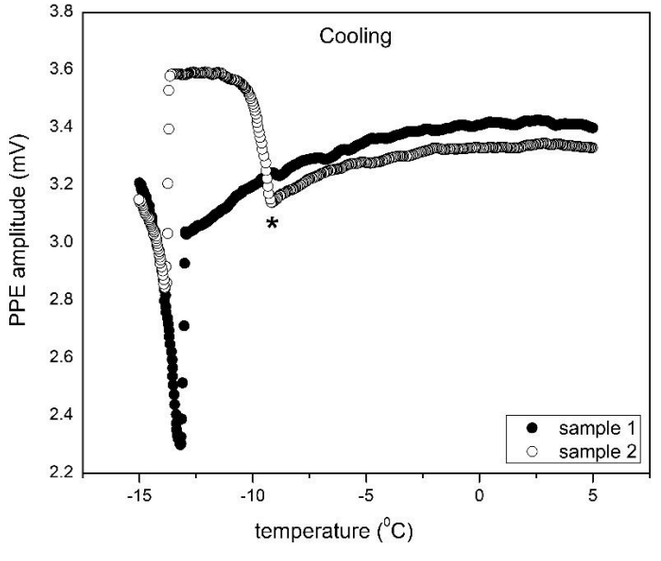

Fig. 46. PPE amplitude as a function of temperature for the RJ samples under investigation, in a temperature range including the freezing point.

Fig. 45 shows that during the heating procedure the amplitude of the PPE signal displays critical anomalies typical for melting processes. Concerning the specific temperature of these anomalies, for sample 1 the anomaly appears at 0˚C and for sample 2 it appears at a lower temperature (around -2˚C). During the cooling procedure the phase transition anomalies appear at much lower temperatures due to the well-known undercooling phenomenon. All four samples present anomalies at around -13˚C, but sample 1 is involved in a second phase transition at a higher temperature (around -10˚C). Chemical analysis indicates that both samples have a similar composition (similar water and sugar content). The only explanation is that for the samples involved in two phase transitions, a coexistence of two different phases (probably free and water-bound) is present. In conclusion, the PPE method, used in a temperature scan arrangement, offers structural information simply by detecting first order phase transitions.

4.3.3(b). Second order phase transitions

Ferroelectric – paraelectric phase transitions

Mandelis et al. were the first to apply the PPE method to ferromagnetic materials, in the detection of a ferro-paraelectric phase transition in Seignette salt.[2] We present an application of the PPE technique to detect ferroelectric-paraelectric phase transitions in another very well-known and intensively studied ferroelectric crystal: triglycine sulphate (TGS). TGS is a ferroelectric crystal with a Curie temperature at about 49 ^{0}C.[126] The interest in its thermal properties is connected to its pyroelectric properties: in the ferroelectric phase, TGS has often been used as a pyroelectric sensor.[114]

When investigating the phase transition of TGS for the purpose of studying the critical behavior of thermal parameters, one must use the back configuration, with the TGS crystal in the front position (directly irradiated), in intimate thermal contact (through a thin coupling fluid) with a pyroelectric sensor ($LiTaO_3$ or PZT). In experimental conditions of opaque and thermally thick samples and thermally thick sensors, the amplitude and phase of the PPE signal are given by Eqs. (7) and (9). Inspection of Eqs. (7) and (9) leads to the conclusion that it is possible to obtain the temperature behavior of all four thermal parameters, from a single measurement, if we have an isolated value of one thermal parameter (other than thermal diffusivity), to calibrate the amplitude measurement. Two other important features should be mentioned: (i) the amplitude of the PPE signal is attenuated by an exponential factor as a_mL_m increases; (ii) the sensitivity of the signal amplitude to changes in the thermal diffusivity is given by the ratio:

$$\frac{dV}{V} / \frac{d\alpha_m}{\alpha_m} = -\frac{a_m L_m}{2} \tag{39}$$

showing that for $a_mL_m>2$, a given anomaly in the thermal diffusivity produces an enhanced signal anomaly. For a given sample, one can adjust the modulation frequency and/or sample thickness, in order to achieve optimal trade-off between sensitivity and signal-to-noise ratio.

Typical temperature scans of the amplitude and phase of the PPE signal in a temperature range including the Curie point of TGS, are displayed in Figs. 47 and 48.

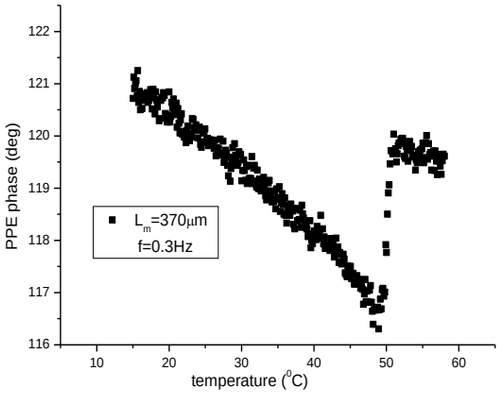

Fig. 47. Temperature scan for the phase of the PPE signal for TGS around the Curie temperature.[128] Reproduced with permission from Dorin, D.; Stephane, L.; Sahraoui, H. Characterization of Ferroelectric Materials by Photopyroelectric Method. In Ferroelectrics - Characterization and Modeling; InTech, https://doi.org/10.5772/19294 2011; licensed under a Creative Commons Attribution (CC BY) license.

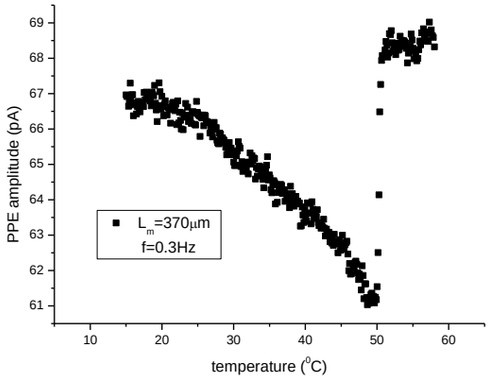

Fig. 48. Temperature scan for the amplitude of the PPE signal for TGS around the Curie temperature. [128] Reproduced with permission from Dorin, D.; Stephane, L.; Sahraoui, H. Characterization of Ferroelectric Materials by Photopyroelectric Method. In Ferroelectrics - Characterization and Modeling; InTech, https://doi.org/10.5772/19294 2011; licensed under a Creative Commons Attribution (CC BY) license.

Using Eqs. (7) and (9), and the well-known relationship between the thermal parameters, one gets the critical behavior of all four thermal parameters (Fig. 49).

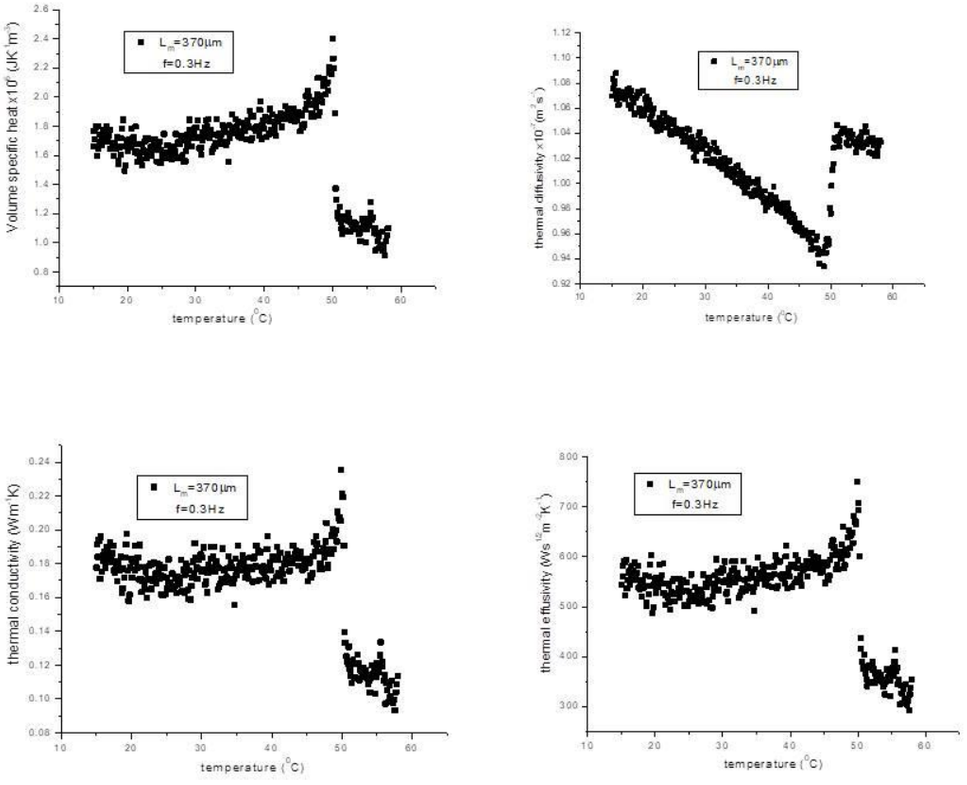

Fig. 49. Temperature behavior of the volume specific heat, thermal diffusivity, conductivity and effusivity of TGS around the Curie point.[128] Reproduced with permission from Dorin, D.; Stephane, L.; Sahraoui, H. Characterization of Ferroelectric Materials by Photopyroelectric Method. In Ferroelectrics - Characterization and Modeling; InTech, https://doi.org/10.5772/19294 2011; licensed under a Creative Commons Attribution (CC BY) license.

One of the most important features concerning the use of the PPE technique for phase transitions investigations is the possibility of enhancing the critical anomaly of the PPE signal, by appropriate handling of the chopping frequency and sample's thickness.

Results from an experiment on a TGS crystal with two different thicknesses (230 µm and 500 µm), investigated at different frequencies (6 Hz and 25 Hz) is displayed in Fig. 50. In this experiment a 1 mm thick PZT ceramic pyroelectric sensor was used.

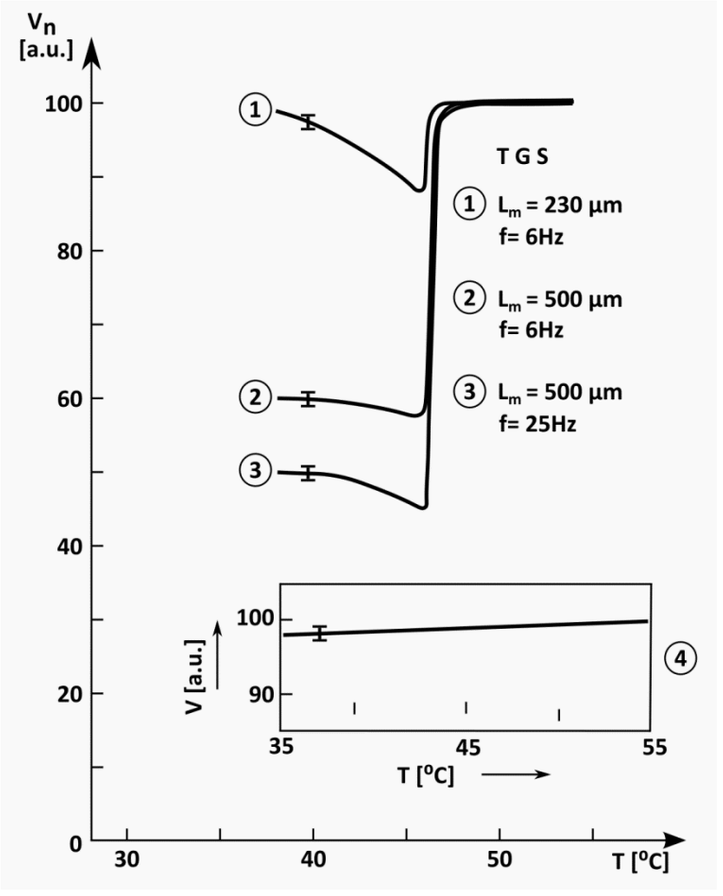

Fig .50. Normalized PPE amplitude as a function of temperature for two TGS single crystals, and for two different chopping frequencies (different thermal diffusion length). Insert: the PPE signal obtained with empty sensor.[129] Reproduced with permission from Appl. Phys. A Solids and Surfaces, 1990, 50 (4), 357 (1990). Copyright 1990 Springer Science+Business Media publishing.

Fig. 50 indicates that the critical anomaly of the PPE amplitude, $\Delta V/V$, increases from 0.14 up to 1.22 with increasing $a_m L_m$, for the same critical anomaly (a jump of about 0.2 in the specific heat). This conveys the suitability of the method towards studies of phase transitions with small critical anomalies of thermal parameters.

Magnetic phase transitions

Magnetic phase transitions were most commonly studied with the purpose of calculating the critical exponents of thermal parameters and to validate existing theories concerning critical phenomena. One of the most studied systems has been Cr_2O_3 involved in an antiferromagnetic-paramagnetic phase transition at about 35 $^{\circ}$C [11] . Ref. [11] describes in detail the procedure of PPE investigations and how to correctly calculate critical exponents. In this tutorial we will present only some general results obtained on this subject: the temperature behavior of the static and dynamic thermal parameters in a temperature region including the Neel temperature (Fig. 51). The system used in this example was in back configuration and the pyroelectric sensor was a $LiTaO_3$ single crystal.

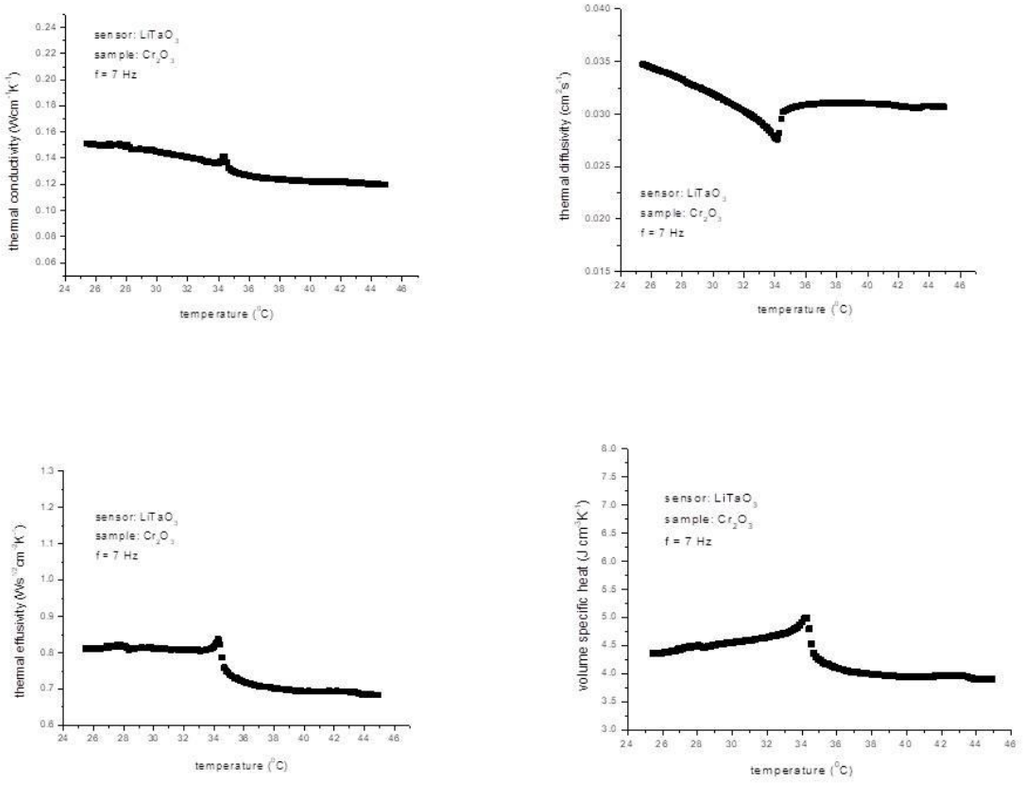

Fig. 51. The temperature behavior of the thermal diffusivity, conductivity, effusivity and volume specific heat of Cr_2O_3 in a temperature range including the Néel point as obtained with PPE method. [128] Reproduced with permission from Dorin, D.; Stephane, L.; Sahraoui, H. Characterization of Ferroelectric Materials by Photopyroelectric Method. In Ferroelectrics - Characterization and Modeling; InTech, https://doi.org/10.5772/19294 2011; licensed under a Creative Commons Attribution (CC BY) license.

As expected, all thermal parameters present anomalies at the Neel point, typical for second order phase transitions.

Fig. 52 presents results obtained in the critical region of the ferro-paramagnetic phase transition of $Ni_{70}Cu_{30}$ alloy.

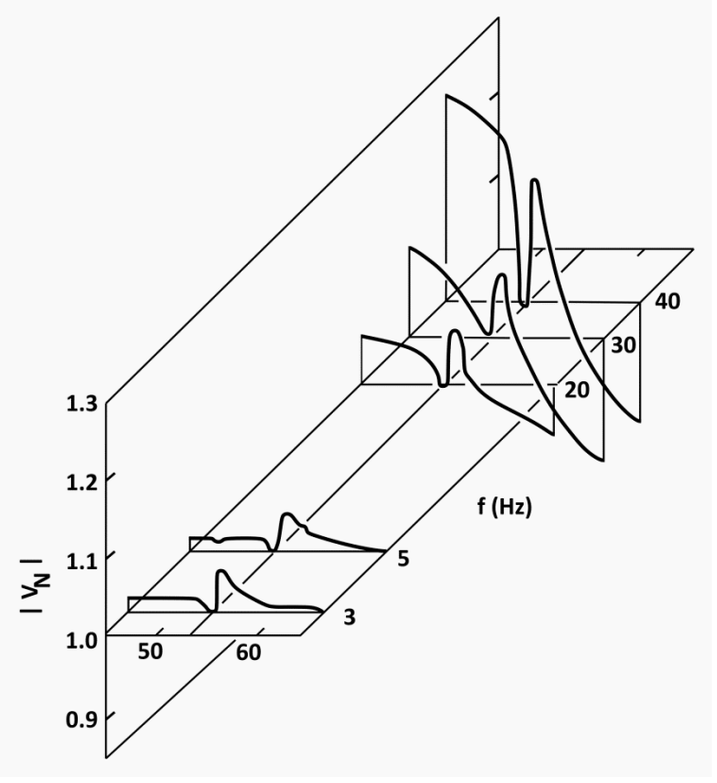

Fig. 52. Normalized amplitude of the PPE signal for a magnetic $Ni_{70}Cu_{30}$ alloy for different values of chopping frequency. The critical anomaly increases with increasing chopping frequency.[130] Reproduced with permission from J. Phys. Chem. Solids, 51(12), 1369 (1990). Copyright 1990 Elsevier.

This application demonstrates a similar principle to the case of ferroelectric materials: by proper selection of the experimental parameters (sample thickness and chopping frequency) one can amplify the critical anomaly of the signal.

At this stage of the tutorial it is probably useful to compare the performances of the PPE technique in detecting phase transitions, with other photothermal techniques. Such a comparison between PPE and the photoacoustic (PA) method is described in Ref. [103]. Following the phase channels for the two methods, in specific cases[11, 110], we obtain the equations:

$$\Theta_{PA} = \tan^{-1}\left(-1-2/p\right);\ p = \beta_s\left(2\alpha_s/\omega\right)^{1/2} \tag{39}$$

for PA phase, and

$$\Theta_{PPE} = -\tan^{-1}\left(\omega\tau_e\right)-1/q\,;\ q = \left(1/L_s\right)\left(2\alpha_s/\omega\right)^{1/2} \tag{40}$$

for PPE phase.

The sensitivity of the two techniques to changes in p and q, respectively, are:

$$\left(\frac{d\Theta}{dp}\right)_{PA} = \left(p^2+p+2\right)^{-1} \tag{41}$$

$$\left(\frac{d\Theta}{dq}\right)_{PPE} = q^{-2} \tag{42}$$

Analysis of Eqs. (41) and (42) leads to the conclusion that the maximum sensitivity of the PA technique is reached when p=0 and has the value ½. Concerning the sensitivity of the PPE technique, it can go (at least theoretically) to infinity.

To conclude this section, we want to make some remarks concerning the temperature behavior of the pyroelectric sensor's properties. Investigations of phase transitions are based on temperature scans, and during a phase transition the measurements of properties of both the sample and sensor change. Fig. 50 contains as an example (inset) where the PPE signal was obtained with an empty sensor over the investigated temperature range. It is clear that the pyroelectric properties of the sensor change monotonically and very little as a function of temperature. For example, for a $LiTaO_3$ sensor, if the investigation is performed far enough from the Curie point of the sensor (about 300 ˚C), the PPE signal increases by about 1% as a function of temperature. Conversely, in the critical region of a phase transition, the sample's properties (i.e., thermal parameters) display sharp anomalies and the critical region is usually rather narrow (a few degrees). Consequently, a small, monotonic change in sensor properties does not significantly influence the results (the critical behavior of the sample's thermal parameters), and usually no normalization procedures are required. It is important that studies are conducted far enough from the Curie temperature of the sensor.

5. CONCLUDING REMARKS

In this tutorial we have attempted to create a picture of how the PPE technique has developed over the past 35 years. In order to remain practical and educational, this paper was organized in three main sections (preceded by an **Introduction** and followed by a **Conclusion** sections). The first two main sections describe the development of the theoretical assumptions and experimental set-ups of the PPE method. The third section is devoted to applications, where of the hundreds of applications available, we selected only a small set that we consider most relevant to convey the breadth of potential that PPE techniques offer.

From a theoretical point of view, it is well-known that the general expression of the complex PPE signal can be calculated exactly, (independent of the composition of the detection cell including the number of layers, the thermal and optical thickness of the layers, etc.) by solving a system of thermal diffusion equations with boundary conditions of flux and temperature continuity at the interfaces of the layered detection cell. However, the mathematical expression of the PPE signal is very complicated and practically useless for most applications. This is why a large effort was dedicated to simplifying it, focusing on the number of components of the detection cell and on the thermal and optical thickness of each layer. In this tutorial, we described several specific cases of experimental interest. The cases reflect the available combinations of the detection configuration, the source of information, scanning parameters and the goal of the measurement.

It should be noted that the theory presented in this tutorial assumes 1D heat propagation through the layers of the detection cell. This restriction seems to be easily satisfied from an experimental point of view. However, theories involving 2D and 3D heat propagation have also been developed.

The main PPE detection configurations used in PPE experiments were originally termed "back" and "front" depending on the relative position of the sensor-incident radiation. For spectroscopic applications a so called "reflection mode" configuration has also been used.

Concerning the detection configuration, the back mode has been more exploited, because it can result in complete thermal characterization (measurement of the thermal diffusivity and effusivity and calculation of the remaining thermal conductivity and volume specific heat) of the sample. The front configuration allows the direct measurement of only the thermal effusivity.

Concerning the source of information, both amplitude and phase of the complex PPE signal can be used. However, the "competition" of PPE amplitude vs phase as a source of information seems to be won by the latter, even if both often result in the same accuracy of results. It is more convenient to measure the phase of the signal, because the phase represents only a time delay of the signal, as compared to a reference one, and it is not dependent on power fluctuations of the incident radiation or on the quality of the incident surface (as is the case with the amplitude).

Many detection schemes have been proposed for investigating thermal parameters of condensed matter samples. Some of them are based on measurements of single values (fixed chopping frequency and sample thickness), others on scanning procedures. This latter type of investigations is clearly more accurate. Two scanning parameters can be used: the chopping frequency of incident radiation and/or the thickness of one of the liquid layers (the sample or coupling fluid) of the detection cell. Each scanning procedure has its advantages and limitations. Frequency scanning is very simple as a procedure, but for accurate results one must know the thickness of all layers of the detection cell. If the scanning procedure is developed over a large frequency range, various layers of the detection cell can pass from a thermally thin to a thick regime, in an uncontrolled way and consequently, theoretical restrictions may be violated. The thickness scanning procedure (performed at constant chopping frequency) does not have the problems mentioned above. Exact knowledge of the liquid layer is not needed because thickness variation can be controlled. However for the TWRC method, the experimental set-up is rather complicated: it must contain 6-axis micrometric stages, nano-motors, etc.

Concerning the "targets" of the measurements, both thermal diffusivity and effusivity can be obtained using the PPE amplitude and phase as source of information. If in a thermal effusivity measurement at least one calibration procedure is involved, a normalization technique is not always necessary when thermal diffusivity measurements are performed. When the thermal diffusivity is deduced from the slope of the amplitude or phase as a function of sample thickness, no calibration is required. In many cases measurement of thermal effusivity is conditional upon knowledge of thermal diffusivity. The final resolution is always better for thermal diffusivity. It is known that the four thermal parameters are connected by two relationships. Consequently, the direct measurement of two of them leads automatically to the possibility of calculating the remaining two (thermal conductivity and volume specific heat). In order to achieve this complete thermal characterization of a sample, one must use the back detection configuration, collecting information from both amplitude and phase, or they must combine two specific cases in back and front configuration.

When considering experimental aspects, the set-ups, detection cells and sensor/sample assemblies described in this tutorial are only examples. The reader can find other experimental solutions in the extended list of references. From experimental point of view it is important to select experimental parameters in such a way that the constraints of the theory are respected during the whole measurement.

At this stage it is probably useful to recommend some of the most suitable parts of a PPE set-up, in the light of the available technologies. Concerning radiation sources, for PPE spectroscopy, the best sources depend on the wavelength of interest. The source can be a Globar or Nernst source, a UV lamp or a tunable diode laser, depending at what wavelength you want to obtain the information. For PPE calorimetry, lasers with a power in the range 5mW – 200mW

are recommended. It is well-known that the intensity of the absorbed radiation must be rather low, in order to keep valid the linear dependence of the PPE voltage as a function of the pyroelectric coefficient (if the intensity of irradiation is too high, non-linear effects can appear). Concerning the modulation of the incident radiation, PPE spectroscopy is usually performed with electro-mechanical choppers which introduces a limitation to the frequency range, especially in the low regime ($f \leq 2$ Hz). For PPE calorimetry, the best modulation is performed electronically, directly from the power supply of the laser. In such a way the frequency range can be extended from 10^{-3} Hz to 10^{5} Hz. Opto-acoustical modulators may also be a solution (they can be used together with lasers for large frequency ranges), but the user must be aware that such a modulator cuts about 25% - 50% from the incident power of the laser. Concerning pyroelectric sensors, the best available, in our opinion, is the z-cut LiTaO3 single crystal; it has a good pyroelectric coefficient, a high Curie temperature, very stable and reproducible thermal and electrical properties and can be obtained from producers as slices of 50µm - 500 µm thickness. Occasionally, PVDF foils (10µm - 50 µm thickness) can be used as pyroelectric sensors, especially when thermally thin sensors are required by the experiment, but the user must be aware that the Curie point of such a sensor is rather low (around 100˚C). PZT ceramics constitute another class of pyroelectric sensors, with a rather good pyroelectric coefficient and rather high Curie temperature, but, unfortunately, their thermal and electrical properties are not stable over time. In the past, some authors have also used triglycine-sulphate (TGS) as a pyroelectric sensor, due to its large pyroelectric coefficient but, unfortunately, the applications for which TGS is suitable are limited due to its low Curie point (around 49˚C) and its hygroscopicity.

PPE signal processing is always performed with lock-in amplifiers. In principle any type of double-phase lock-in amplifier is suitable for signal processing. Such amplifiers have in-built preamplifiers of 10^{6} Ω or 10^{8} Ω. When necessary, additional preamplifiers of larger electrical resistivity can be used. Current or voltage mode types of measurement can be selected experimentally, depending on the application. For PPE spectroscopy, an important part of the set-up is the monochromator. Though their resolution can be limited, we suggest that the most suitable option for PPE experiments are prism monochromators; our main reason is that they let enough energy reach the detection cell. Due to the fact that PPE spectroscopy is usually one-channel spectroscopy, a degree of normalization is always necessary; blackened $LiTaO_3$ can be used as sensor for normalization.

Selecting the applications to present in this tutorial was a significant challenge. As already mentioned, in over 35 years of development, the PPE technique has proven itself to be useful in many types of application. We stress the idea that the PPE method can be applied for thermal characterization of practically all types of condensed matter materials: liquids (simple and volatile liquids, binary and isotopic mixtures, magnetic nanofluids, (semi)liquid foodstuffs -oils, margarines, juices, honey, meat, cheese, starch -, blood, etc.) and solids (thermal and electrical good or bad conductors, ferroelectrics, pyroelectrics, thermoelectrics, magnets, composites as dental or building materials, etc.). To the best of our knowledge, the only types of sample that cannot be investigated by PPE are chemically aggressive (acids for example). Liquids are the best samples for investigation as the thermal contact liquid sample/solid pyroelectric sensor is ideal. As mentioned, when investigating solids, a coupling fluid between the solid sample and the solid pyroelectric sensor can influence quantitative data. However, due to the effort of several groups, during the last decade the influence of the coupling fluid on results has been reduced or in certain cases eliminated. A recent success story in the development of this technique is the ability to investigate, with high accuracy, porous solids. It is important to note that, for all types of PPE investigation, a small quantity of material (µl or mg) is required. The possibility of using a small quantity of sample is of great importance when

investigating rare and/or expensive samples such as isotopic liquid mixtures, magnetic nanofluids, itinerant electron antiferromagnetic materials, high Tc superconductors, etc.

One of the purposes of presenting the applications described in this tutorial was to demonstrate that physical and chemical processes such as molecular and isotopic associations, vegetable oils spoilage and adulteration or phase transitions, can be studied by PPE calorimetry, provided accurate measurements are performed. In fact, high-resolution PPE calorimetry is able to investigate any process associated with small changes in static and dynamic thermal parameters. Of all of the applications to which PPE is suited, in our opinion special attention should be placed in phase transition detection. PPE is one of the most powerful techniques for phase transition investigations. Both first and second order phase transitions have been investigated by PPE and the behavior of all static and dynamic thermal parameters in the phase transition region has been obtained. Concerning first order phase transitions, melting (vaporization, freezing) points have been detected and the hysteresis of heating-cooling cycles have been observed. This information has been used to study various processes such as oil adulteration and honey hygroscopicity. Concerning second order phase transitions (due to the possibility offered by advanced PPE experimental set-ups which allow very slow temperature variation rates), the behavior of thermal parameters in very narrow critical regions (antiferromagnetic – paramagnetic, ferroelectric – paraelectric, phase transitions taking place in liquid crystals or liquid thermoelectrics) has been obtained. Even more, critical exponents for thermal parameters have been measured proving the suitability of the PPE method in fundamental physics research (critical exponents are universal numbers).

The PPE method is an example of absorption spectroscopy and consequently it appears to be useful in the investigation of strongly absorbing materials (solids and liquids). For such types of materials classical two channels transmission spectroscopy is useless. As a recent result, PPE spectroscopy was successfully used to obtain both spectroscopic and calorimetric information on strongly absorbing solids (semiconductors). A weakness to this is that it is a one channel method, so it needs normalization procedures and for classical (semi-transparent) samples, classical two-channels differential spectroscopies are more often performed.

Finally, we would like to point out that almost all of the results described in this tutorial belong to our group, together with our co-workers. We hope that the readers and the members of other groups active in this field understand the reason behind this limitation (i.e., there would be too much information to be included in a single paper). However, we are confident that the extended list of references will provide useful to access the results of other groups.

Acknowledgements
This work is funded by the Romanian Ministry of Research, Innovation and Digitalisation through Programme NUCLEU, Contract No. PN19 35 02 01 and by Slovenian Research Agency within the project "Synthesis and characterization of sporopollenine-based biocomposite materials with biocidal activity against antibiotic-resistant microorganisms" (J7-2602). Technical assistance from M. Bojan is also acknowledged.

Author Declarations
The authors have no conflict of interests to disclose. This research article does not contain experiments on animals and/or human subjects.

Data Availability Statement
The data that supports the findings of this study are available within the article.

References

1. A. C. Tam, Rev. Mod. Phys. **58**, 381 (1986).

2. A. Mandelis, Chem. Phys. Lett. **108**, 388 (1984).

3. D. Dadarlat, M. Chirtoc, R. M. Candea, and I. Bratu, Infrared Phys. **24**, 469 (1984).

4. H. Coufal, Appl. Phys. Lett. **44**, 59 (1984).

5. S. B. Lang, Ferroelectrics **7**, 231 (1974).

6. A. Mandelis, Rev. Sci. Instrum. **82**, 120901 (2011).

7. A. Mandelis, and M. M. Zver, J. Appl. Phys. **57**, 4421 (1985).

8. M. Chirtoc, and G. Mihailescu, Phys. Rev. B **40**, 9606 (1989).

9. D. Dadarlat, D. Bicanic, H. Visser, F. Mercuri, and A. Frandas, J. Amer. Oil Chem. Soc., **72**, 281 (1995), Springer Nature. https://doi.org/10.1007/BF02541083

10. K. Strzałkowski, and D. Dadarlat, Measurement **184**, 109956 (2021).

11. M. Marinelli, F. Mercuri, U. Zammit, R. Pizzoferrato, F. Scudieri, and D. Dadarlat, Phys. Rev. B **49**, 9523 (1994).

12. D. Dadarlat, M. Chirtoc, C. Neamtu, R. Candea, and D. Bicanic, Phys. Stat. Sol. **(a)121**, K231 (1990).

13. D. Dadarlat, and A. Frandas, Appl. Phys. **A56**, 235 (1993).

14. M. Chirtoc, D. Dadarlat, I. Chirtoc, and D. Bicanic, Spectroscopy Lett. **21**, 413 (1988).

15. D. Dadarlat, H. Visser, and D. Bicanic, Meas. Sci. Technol. **6**, 1215 (1995).

16. A. Mandelis, and A. Matvienko, Pyroelectric Materials and Sensors, D. Remiens (Ed.), Kerala, India, 61 (2007).

17. J. Shen, A. Mandelis, and H. Tsai, Rev. Sci. Instrum. **69**, 197 (1998).

18. A. Salazar, A. Oleaga, A. Mendioroz, and E. Apiñaniz, Measurement **121**, 96 (2018)

19. S. Delenclos, M. Chirtoc, A. Hadj Sahraoui, C. Kolinsky, and J. M. Buisine, Rev. Sci. Instrum. **73**, 2773 (2002).

20. J. Shen, and A. Mandelis, Rev. Sci. Instrum. **66**, 4999 (1995).

21. D. Dadarlat, C. Neamtu, E. Surducan, A. Hadj Sahraoui, S. Longuemart, and D. Bicanic, Instr. Sci. Technol. **30**, 387 (2002).

22. C. Neamtu, D. Dadarlat, M. Chirtoc, A. Hadj Sahraoui, S. Longuemart, and D. Bicanic, Instr. Sci. Technol. **34**, 225 (2006).

23. A. Sikorska, D. Dadarlat, B. B. J. Linde, M. Streza, C. Neamtu, and A. Sliwinski, J. Phys. IV **137**, 341 (2006). DOI: 10.1051/jp4:2006137065

24. J. A. Balderas-Lopez, A. Mandelis, and J. A. Garcia, Rev. Sci. Instrum. **71**, 2933 (2000).

25. J. A. Balderas-Lopez, and A. Mandelis, Rev. Sci. Instrum. **74**, 700 (2003).

26. C. Gu, J. Shen, J. Zhou, K. H. Michaelian, R. Gieleciak, N. G. C. Astrath, and M. L. Baesso, Rev. Sci. Instr. **90**, 014901 (2019).

27. E. Marín, and H. Vargas, Recent developments in thermal wave interferometry for gas analysis, in Thermal Wave Physics and Related Photothermal Techniques: Basic Principles and Recent Developments, E. M. Moares (Ed.), Transworld Research Network, Kerala, India, (2009).

28. A. Mandelis, and A. Matvienko, Photopyroelectric thermal-wave cavity devices–10 years later, in Pyroelectric Materials and Sensors, D. Rémiens (Ed.), Research Signpost, Kerala, India, (2007).

29. D. Dadarlat, C. Neamtu, V. Tosa, and M. Streza, Acta. Chim. Slov. **54**, 149 (2007).

30. D. Dadarlat, and C. Neamtu, Acta. Chim. Slov. **56**, 225 (2009).

31. D. Dadarlat, Laser Phys. **19**, 1330 (2009). https://doi.org/10.1134/S1054660X09060255

32. D. Dadarlat, C. Neamtu, N. Houriez, S. Delenclos, S. Longuemart, and A. Hadj Sahraoui, Eur. Phys. J. Special Topics **153**, 115 (2008).

33. D. Dadarlat, and C. Neamtu, Meas. Sci. Technol. **17**, 3250 (2006).

34. D. Dadarlat, M. Bicazan, A. Frandas, V. V. Morariu, A. Pasca, H. Jalink, and D. Bicanic, Instr. Sci. Technol. **25**, 235 (1997).

35. S. Longuermart, A. Hadj Sahraoui, D. Dadarlat, S. Delenclos, C. Kolinsky, and J. M. Buisine, Rev. Sci. Instrum. **74**, 805 (2003).

36. A. Hadj Sahraoui, S. Longuemart, D. Dadarlat, S. Delenclos, C. Kolinsky, and J. M. Buisine, Ferroelectrics **289**, 97 (2003).

37. H. Jalink, A. Frandas, R. Van der Schoor, and D. Bicanic, Rev. Sci. Instrum. **67**, 3990 (1996).

38. K. Strzałkowski, D. Dadarlat, M. Streza, and F. Firszt, Thermochim. Acta **614**, 232 (2015).

39. A. Salazar, and A. Oleaga, Rev. Sci. Instrum. **83**, 014903 (2012).

40. A. Salazar, Rev. Sci. Instrum. **74**, 825 (2003).

41. U. Zammit, F. Mercuri, S. Paoloni, M. Marinelli, and R. Pizzoferrato, J. Appl. Phys. **117**, 105104, 1 (2015).

42. C Tripon, N. Cobirzan, A. A. Balog, R. Fechete, R. Gutt, D. Dadarlat, U. Zammit, F. Mercuri, and S. Paoloni, Thermochim. Acta. **702,** 178943 (2021). https://doi.org/10.1016/j.tca.2021.178943

43. D. Dadarlat, M. N. Pop, M. Streza, S. Longuemart, M. Depriester, A. Hadj Sahraoui, and V. Simon, Int. J. Thermophysics **31**, 2275 (2010). https://doi.org/10.1007/s10765-010-0854-1

44. D. Dadarlat, M. N. Pop, M. Streza, S. Longuemart, M. Depriester, A. Hadj Sahraoui, and V. Simon, Int. J. Thermophysics **32**, 2092 (2011). https://doi.org/10.1007/s10765-011-1067-y

45. D. Dadarlat, J. Therm. Analysis Calor. **110**, 27 (2012).

46. M. Kuriakose , M. Depriester, R. C. Y. King, F. Rousel, and A. Hadj Sahraoui, J. Appl. Phys. **113**, 044502 (2013).

47. D. Dadarlat, M. Streza, R. C. Y. King, F. Roussel, M. Kuriakose, M. Depriester, E. Guilmeau, and A. Hadj Sahraoui, Meas. Sci. Technol. **25** 015603 (2014).

48. M. Bonetti, S. Nakamae, M. Roger, and P. Guenoun, J. Chem. Phys. **134**, 114513 (2011).

49. K. Touati, M. Depriester, M. Kuriakose, and A. Hadj Sahraoui, Rev. Sci Instr. **86,** 094901 (2015).

50. K. Touati, M. Depriester, A. H. Sahraoui, C. Tripon, and D. Dadarlat, Thermochim. Acta **624,** 21 (2016).

51. D. Dadarlat, P. R. N. Misse, A. Maignan, E. Guilmeau , R. Turcu, L. Vekas, C. Tudoran, M. Depriester, and A. Hadj Sahraoui, Int. J. Thermophys. **36**, 244 (2015).

52. D. Dadarlat, E. Guilmeau, A. Hadj Sahraoui, C. Tudoran, V. Surducan, C. Bourgès, and P. Lemoine, Int. J. Thermophys. **37**, 53 (2016).

53. D. Dadarlat, C. Tripon, and V. Tosa, Thermochim. Acta **653**, 133 (2017).

54. K. Strzałkowski, M. Streza, D. Dadarlat, and A. Marasek , J. Therm. Analysis. Calor. **119**, 319 (2015).

55. K. Strzałkowski, D. Dadarlat, M. Streza, and J. Zakrzewski, Appl. Phys. A **119,** 1165 (2015).

56. D. Bicanic, M. Streza, O. Dóka, D. Valinger, S. Luterotti, Zs. Ajtony, Z. Kurtanjek, and D. Dadarlat, Int. J. Thermophys. **36**, 2380 (2015).

57. N. Cobarzan, A. A. Balog, B. Belean, G. Borodi, D. Dadarlat, and M. Streza, Construction & Building Materials **105**, 297 (2016).

58. M. Depriester, P. Hus, S. Delenclos, and A. Hadj Sahraoui, Rev. Sci. Instrum. **76**, 074902 (2005).

59. M. Depriester, A. Hadj Sahraoui, P. Hus, and F. Roussel, Appl. Phys. Lett. **94**, 231910 (2009).

60. A. Mandelis, Diffusion-Wave Fields: Mathematical Methods and Green Functions, Springer (Ed.), New-York, 148 (2001).

61. D. Lupu, M. Chirtoc, D. Dadarlat, R. Candea, I. Bratu, and V. Mecea, Phys. Stat. Sol. (b) **163**, 519 (1991).

62. E. H. Bentefour, C. Glorieux, M. Chirtoc, and J. Thoen, J. Appl. Phys. **93**, 9610 (2003).

63. H. Jalink, A. Frandas, R. van der Schoor, and D. Bicanic, Rev. Sci. Instrum. **67**, 3990 (1996).

64. S. Paoloni, U. Zammit, and F. Mercuri, Int. J. Thermophys. **39**, 33 (2018).

65. S. Paoloni, F. Mercuri, and U. Zammit, J. Chem. Phys. **145**, 124506 (2016).

66. U. Zammit, F. Mercuri, S. Paoloni, M. Marinelli, and R. Pizzoferrato, Molecular Crystals and Liquid Crystals **614**, 128 (2015).

67. U. Zammit, F. Mercuri, S. Paoloni, M. Marinelli, and R. Pizzoferrato, J. Appl. Phys. **117**, 105104 (2015).

68. S. Paoloni, U. Zammit, M. Marinelli, F. Mercuri, and R. Pizzoferrato, Review of Scientific Instruments **84**, 054904 (2013).

69. U. Zammit, S. Paoloni, F. Mercuri, M. Marinelli, and F. Scudieri, AIP Advances **2**, 012135 (2012).

70. U. Zammit, M. Marinelli, F. Mercuri, S. Paoloni, and F. Scudieri, Rev. Sci. Instrum. **82**, 121101 (2011).

71. P. Menon, R. Rajesh, J. Thoen, and C. Glorieux, Thermal Conductivity 30: Thermal Expansion 18 Book Series Thermal Conductivity 30, 920 (2010).

72. M. Chirtoc, F. Brizion, and I. Chirtoc, Journal De Physique IV **125**, 661 (2005).

73. D. Dadarlat, and C. Neamtu, Recent Development of Photopyroelectric Calorimetry of Liquids**,** in Thermal wave physics and related photothermal techniques: Basic principles and recent developments, Ernesto Morales Marin (Ed.), Kerala, India, 65 (2009).

74. U. Zammit, M. Marinelli, F. Mercuri, S. Paoloni, and F. Scudieri, Rev. Sci. Instrum. **82**, 121101 (2011).

75. R. M. Candea, D. Lupu, M. Chirtoc, D. Dadarlat, and A. Frandas, Spectroscopy Lett. **26**, 923 (1993).

76. D. Dadarlat, A. Frandas, and I. Bratu, Infrared Phys. **33**, 575 (1992).

77. D. Dadarlat, C. Neamtu, R. Pop, M. Marinelli, and F. Mercuri, J. Optoelectron. Adv. Mat. **9,** 2847 (2007).

78. A. Salazar, A. Oleaga, A. Mendioroz, and E. Apinaniz, Measurement Science And Technology **28**, 105011 (2017).

79. S. Pittois, M. Chirtoc, C. Glorieux, W. van den Bril, and J. Thoen, Analytical Sci. (Japan) **17**, S110 (2001).

80. D. Dadarlat, M. N. Pop, O. Onija, M. Streza, M. M. Pop, S. Longuemart, M. Depriester, A. Hadj Sahraoui, and V. Simon, J. Therm. Analysis Calor. **111**, 1129 (2013). https://doi.org/10.1007/s10973-012-2270-1

81. L. Silaghi-Dumitrescu, D. Dadarlat, M. Streza, T. Buruiana, D. Prodan, I. Hodisan, and C. Prejmerean, J. Therm. Analysis Calor. **118**, 623 (2014). https://doi:10.1007/s10973-013-3561-x

82. D. Dadarlat, M. Streza, O. Onija, K. Strzalkowski, C. Prejmerean, L. Silaghi Dumitrescu, and N. Cobirzan, J. Therm. Analysis Calor. **119**, 301 (2015). https://doi.org/10.1007/s10973-014-4091-x

83. A. Mandelis, Principles and Perspectives of Photothermal and Photoacoustic Phenomena, Elsevier (Ed.), (1992).

84. J. H. Perry, Chemical Engineering Handbook, McGrow-Hill (Ed.), New York, (1963).

85. Y. S. Touloukian, Thermophysical Properties of High Temperatures Solid Materials, MacMillan (Ed.), New York, (1967).

86. D. Dadarlat, Proc. SPIE **8411**, 84110T (2012). https://doi.org/10.1117/12.933860

87. D. Dadarlat, and M. N. Pop, Meas. Sci. Technol. **21**, 105701 (2010). https://doi.org/10.1088/0957-0233/21/10/105701

88. M. Streza, M. N. Pop, K. Kovacs, V. Simon, S. Longuemart, and D. Dadarlat, Laser Phys. **19**, 1340 (2009).

89. A. Hadj Sahraoui, S. Longuermart, D. Dadarlat, S. Delenclos, C. Kolinsky, and J. M. Buisine, Rev. Sci. Instrum. **73**, 2766 (2002).

90. A. Hadj Sahraoui, S. Longuermart, D. Dadarlat, S. Delenclos, C. Kolinsky, and J. M. Buisine, Rev. Sci. Instrum. **74**, 618 (2003).

91. S. Longuermart, A. Hadj Sahraoui, D. Dadarlat, S. Delenclos, C. Kolinsky, and J. M. Buisine, Rev. Sci. Instrum. **74**, 805 (2003).

92. E. H. Bentefour, C. Glorieux, M. Chirtoc, and J. Thoen, Rev. Sci. Instrum. **74**, 811 (2003).

93. A. Hadj Sahraoui, S. Longuemart, D. Dadarlat, S. Delenclos, C. Kolinsky, and J. M. Buisine, Ferroelectrics **289**, 97 (2003).

94. R.W. Whatmore, Rep. Progr. Phys. **49**, 1335 (1986).

95. T. Z. Fullem, and Y. Danon, J. Appl. Phys. **106**, 074101 (2009).

96. E.H. Bentefour, C. Glorieux, M. Chirtoc, and J. Thoen, Rev. Sci. Instrum. **74**, 811(2003).

97. M. Nakamura, S. Takekawa and K. Kitamura, Opt. Mat. **32**, 1410 (2010).

98. D. Dadarlat, S. Longuemart, and A. Hadj Sahraoui, Characterization of Ferroelectric Materials by Photopyroelectric Method, in Ferroelectrics-Characterization and Modeling, M. Lallart (Ed.), INTECH, 281 (2011).

99. A. Cruz-Orea, E. H. Bentefour, P. Jamee, M. Chirtoc, C. Glorieux, G. Pitsi, and J. Thoen, Rev. Sci. Instrum. **74**, 818 (2003).

100. A. Marin-Serrano, J. A. Balderas-Lopez, P. A. Calva, and A. Aranda-Perez, Thermochimica Acta **676**, 33 (2019).

101. J. A. Balderas-Lopez, M. R. Jaime-Fonseca, G. Galvez-Coyt, A. Munoz-Diosdado, J. A. Pescador, J. Diaz-Reyes, and B. E. Chavez-Sandoval, Int. J. Thermophys. **39**, 111 (2018).

102. J. A. Balderas-Lopez, M. R. Jaime-Fonseca, G. Galvez-Coyt, A. Munoz-Diosdado, J. A. Pescador, J. Diaz-Reyes, and B. E. Chavez-Sandoval, Int. J. Thermophys. **39**, 111 (2018).

103. G. A. Lopez-Munoz, and J. A. Balderas-Lopez, Thermochimica Acta **579**, 40 (2014).

104. J. A. Balderas-Lopez, Meas. Sci. and Technol. **23**, 065501 (2012).

105. S. Delenclos, D. Dadarlat, N. Houriez, S. Longuermart, C. Kolinsky, and A. Hadj Sahraoui, Rev. Sci. Instrum. **78**, 024902 (2007).

106. J. A. Eastman, S. U. S. Choi, S. Li, W. Yu, and L.Thomson, J.Appl. Phys. Lett. **78**, 718 (2001).

107. S. U. S. Choi, Z. G. Zhang, W. Yu, F. E. Lockwood, and E. A. Grulke, Appl. Phys. Lett. **79**, 2252 (2001).

108. D. Dadarlat, S. Longuemart, R. Turcu, M. Streza, L. Vekas, and A. Hadj Sahraoui , Int. J. Thermophys. **35**, 2032 (2014). https://doi.org/10.1007/s10765-013-1549-1

109. D. Dadarlat, P. R. N. Misse, A. Maignan, E. Guilmeau, R. Turcu, L. Vekas, C. Tudoran, M. Depriester, and A. Hadj Sahraoui, Int. J. Thermophys. **36**, 2441 (2015). https://doi.org/10.1007/s10765-015-1855-x

110. D. Dadarlat, I. Craciunescu, R. Turcu, and C. Tripon, Int. J. Thermophys. **38**, 86 (2017). https://doi.org/10.1007/s10765-017-2227-5

111. M. Streza, D. Dadarlat, C. Bele, F.V. Dulf, C. Socaciu and V. Simon, Food Biophys. **4**, 147 (2009). Springer Nature. https://doi.org/10.1007/s11483-009-9111-1

112. D. Dadarlat, C. Neamtu, M. Streza, C. Socaciu, C. Bele, and F. Dulf, Europ. J. Lipids. Sci. Tech. (EJLST) **111**, 148 (2009).

113. H.E. Stanley, Introduction to phase transitions and critical phenomena, Oxford University Press, New York, Oxford, (1971).

114. D. Dadarlat, M. Chirtoc, and D. Bicanic, Appl.Phys. **A50**, 357 (1990).

115. D. Dadarlat, M. Chirtoc, C. Neamtu, and D. Bicanic, J. Phys. Chem. Solids **51**, 1369 (1990).

116. D. Dadarlat, A. Frandas, M. Marinelli, F. Mercuri, and D. Bicanic, Appl. Phys. **A61**, 183 (1995).

117. S. Paoloni, F. Mercuri, and U. Zammit, Int. J. Thermophys. **40**, 107 (2019).

118. S. Paoloni, U. Zammit, P. Galloni, and F. Mercuri,https://www.webofscience.com/wos/author/record/2119056 Thermochimica Acta **695**, 178843 (2021).

119. S. Paoloni, F. Mercuri, U. Zammit, J. Leys, C. Glorieux, and J. Thoen, J. Chem. Phys. **148**, 094503 (2018).

120. A. Herrero, A. Oleaga, P. Manfrinetti, A. Provino, and A. Salazar, Intermetallics **101**, 64 (2018).

121. A. Oleaga, V. Shvalya, V. Liubachko, G. Balakrishnan, L. D. Tung, and A. Salazar, J. Alloys and Compounds **703**, 210 (2017).

122. D. Dadarlat, D. Bicanic, J. Gibkes, W. Kloek, I. Dries, and E. Gherkema, Chem. Phys. Lipids **82,** 15 (1996).

123. D. Dadarlat, D. Bicanic, J. Gibkes, V. Surducan, and A. Pasca, J. Food Sci. Agric. **78**, 182 (1998).

124. D. Dadarlat, K. J. Riezebos, D. Bicanic, C. van den Berg, E. Gerkema, and V. Surducan, Adv. Food Sci. **20**, 27 (1998).

125. R. Margaoan, C. Tripon, O. Bobis, V. Bonta, and D. Dadarlat, Analythical Letters **54**, 3 (2021). https://doi.org/10.1080/00032719.2019.1700269

126. J. del Cerro, S. Ramos, and J. M. Sanchez-Laulhe, J. Phys. E: Sci. Instrum. **20**, 612 (1987).

127. U. Zammit, M. Marinelli, F. Mercuri, R. Pizzoferrato, F. Scudieri, and S. Martelucci, J. Phys. E Sci. Instrum. **21**, 935 (1988).

128. D. Dadarlat, L. Stephane and S. H. Abdelhak, Characterization of Ferroelectric Materials by Photopyroelectric Method**,** in Ferroelectrics - Characterization and Modelling, Mickael Lallart (Ed.), Rijeka, Croatia, 281 (2011).

129. D. Dadarlat, M. Chirtoc, D. Bicanic, Appl. Phys. A50, 357 (1990), https://doi.org/10.1007/BF00323590

130. D. Dadarlat, M. Chirtoc, C. Neamtu, D. Bicanic: J. Phys. Chem. Solids **51**, 1369 (1990), https://doi.org/10.1002/pssa.2211210259